Title

Resistance of special-shaped concrete-filled steel tube columns under compression and bending

Authors

Liu, Xianggang
Liu, Jiepeng
Yang, Yuanlong
et al.

Publication Date

2020-06-01

DOI

10.1016/j.jcsr.2020.106038

Resistance of special-shaped concrete-filled steel tube columns under compression and bending

Xianggang Liu [a,b], Jiepeng Liu [a,d], Yuanlong Yang [a,c,d,*], Guozhong Cheng [a,d], Joel Lanning [e]

[a] Key Laboratory of New Technology for Construction of Cities in Mountain Area (Ministry of Education), Chongqing University, Chongqing 400045, China
[b] China Southwest Architectural Design and Research Institute Co., Ltd, Chengdu 610042, China
[c] Key Lab of Structures Dynamic Behavior and Control (Harbin Institute of Technology), Ministry of Education, Harbin 150090, China
[d] School of Civil Engineering, Chongqing University, Chongqing 400045, China
[e] Civil and Environmental Engineering, University of California, Irvine 92617, USA

a r t i c l e i n f o

Article history:
Received 13 October 2019
Received in revised form 1 February 2020
Accepted 13 March 2020
Available online 3 April 2020

Keywords:
Special-shaped column
CFST column
Resistance
Bending
Eccentric compression

a b s t r a c t

Design procedures for L-shaped and T-shaped concrete-filled steel tube (CFST) columns subjected to bending and compression loading scenarios were developed through parametric study using finite element (FE) models verified by existing experimental results. The finite element study on this special-shaped CFST column subjected to pure bending considered parameters of steel-to-concrete ratio α, steel yield strength f_y, concrete strength f_{ck}, and column limb width-to-thickness ratio B/t_w (H/t_w). For their behavior under eccentric compression, additional parameters of section stiffening pattern, loading angel ϑ, eccentricity, and axial compression ratio were included. Parametric analysis results show that steel-to-concrete ratio α, steel yield strength f_y and column limb width-to-thickness ratio B/t_w (H/t_w) have obvious influences on the flexural resistances of the special-shaped CFST columns, while concrete strength f_{ck} has a small effect and can be ignored. The column limb width-to-thickness ratio B/t_w, steel to concrete ratio α, steel yield strength f_y, concrete compressive strength f_{ck}, loading angle ϑ, eccentricity e and section stiffening type have significant effects on the N-M correlation curves, and the convex portion of the N-M curves has a certain symmetry. The column limb width-to-thickness ratio B/t_w and axial compression ratio n have significant effects on the shape of M_x-M_y correlation curves. Based on the FE analysis results, design formulae for calculating sectional flexural resistances were proposed for special-shaped CFST columns. Besides, simplified formulae were provided to conservatively predict the resistances of special-shaped CFST section and column under eccentric compression based on extensive analysis results of FE models.

1. Introduction

The traditional rectangular column has column corners which protrude towards the inside of the rooms (Fig. 1(a)), which not only affects the indoor visual aesthetic, but also reduces the building area [1]. Columns with special-shaped (T-shaped, L-shaped, or cruciform-shaped) cross sections as shown in Fig. 1(b), are possible solutions to undesirable protruding column corners [1]. The width-to-thickness ratio of each column limb is typically not more than 4. Special-shaped columns have been increasingly used in residential and official buildings because of the smooth connection between special-shaped columns and adjacent infilled walls, which can more efficiently utilize indoor floor space.

Previous studies mainly focused on the static behavior of T-shaped and L-shaped reinforced concrete columns subjected to concentric compressive load or biaxial eccentric compressive load, from which moment and axial force interaction relationships for design were proposed [2–7]. Recent studies on special-shaped concrete-filled steel tube (CFST) columns have shown their superior seismic performance is over conventional special-shaped reinforced concrete columns [8–15]. Special-shaped CFST column structure not only has the characteristics of traditional special-shaped column structure, but also has the ability of the steel tube to restrain the core concrete, thus improving its strength and ductility [12,14–16]. Besides, the special-shaped CFST column structure caters to the trend of building assembly and industrialization. Since special-shaped CFST columns have the architectural benefits of special-shaped columns and desirable seismic behavior, many projects have utilized this new type of structural system (see Fig. 2).

Although special-shaped CFST columns have been applied in many practical projects, the existing specifications and regulations, such as Chinese technical specification for concrete structures with specially shaped columns (JGJ149–2017) [1] and technical code for con- crete filled steel tubular structures (GB50936–2014) [17], have no

* Corresponding author at: Key Laboratory of New Technology for Construction of Cities in Mountain Area (Ministry of Education), Chongqing University, Chongqing 400045, China.
E-mail address: yangyuanlong@cqu.edu.cn (Y. Yang).

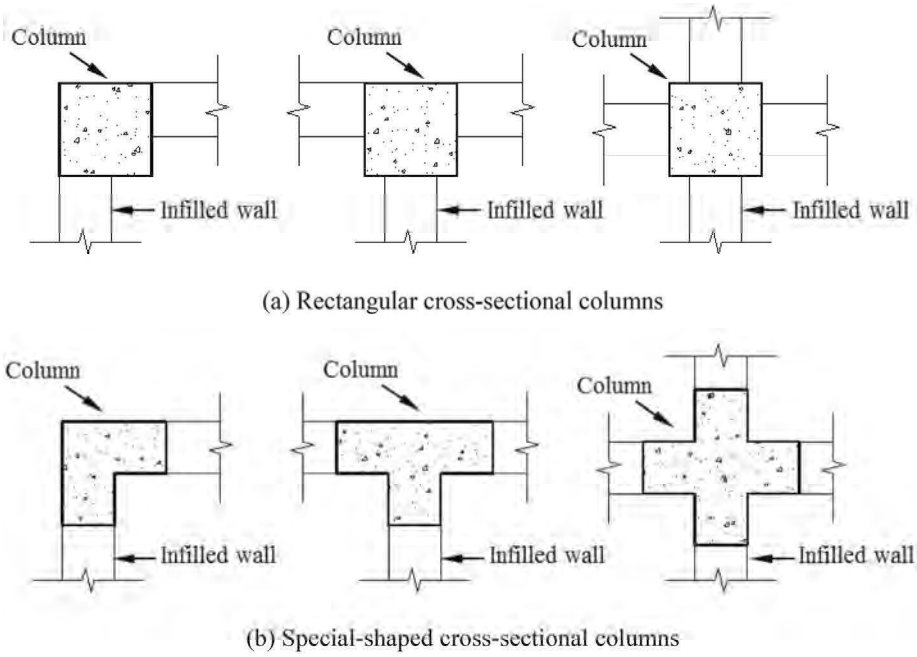

Fig. 1. Rectangular and special-shaped cross-sectional columns in frame structures.

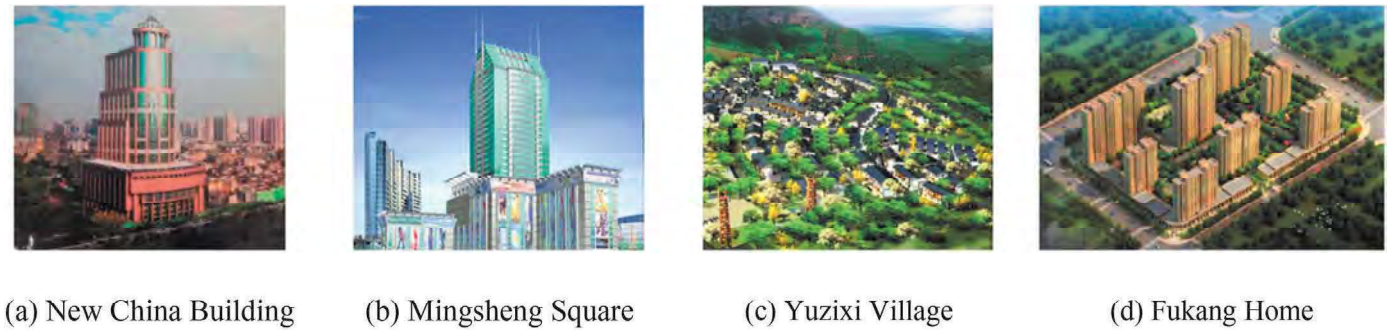

Fig. 2. Applications of special-shaped CFST columns. Note: The images in Fig. 2 from reference [37,38].

established design methods for computing their resistances. Existing studies have focused primarily on numerical simulations [18,19], which are not convenient for engineering design. As so far, some researchers have carried out experimental studies on the performance of special-shaped CFST columns subjected to eccentric compression [18,19], and relatively few studies on its pure bending performance [20]. So, until more experimental studies of special-special CFST columns under both eccentric compression and bending are found, extensive FE analysis could come as rescue to the designers. Besides, the references [12,16,21,23,30,32,35,36] show that the FE software ABAQUS can be used to simulated analysis for CFST columns to obtain results consistent with experiment. Therefore, this paper develops a design procedure for special-shaped CFST columns under pure bending as well as eccentric compression using finite element (FE) models, in the ABAQUS software package, verified against existing experimental results. Parameter analysis was carried out to study the influences of section stiffening measures, loading angel ϑ, column limb width-to-thickness ratio B/t_w, steel-to-concrete ratio α, steel yield strength f_y, concrete prismatic compressive strength f_{ck}, eccentricity e, and axial compression ratio n. The design methods for the resistances of special-shaped CFST columns proposed are convenient for the engineering design practice and are shown to be conservative.

2. Finite element models

The FE models of special-shaped CFST were built in ABAQUS to reflect specimens tested in pure bending by Liu et al. [20] and those subjected to eccentric compression by Yang et al. [18] and Zuo et al. [19]. These test results were used to verify the FE modeling process and to ensure realistic results such that further parametric study could be reliably carried out.

2.1. Material constitutive models and element types

The steel constitutive model used employs an elastic perfectly plastic bilinear stress-strain relationship (Fig. 3(a)) with a small tangent modulus of strain-hardening equal to 1% of the elastic modulus [21–23,32]. The elastic modulus E_s of steel is assumed as 2.06×10^5 MPa, and the Poisson's ratio of steel is 0.3.

The plastic damage constitutive model is adopted for concrete [21–27]. Five parameters in this concrete constitution describe its yield function and plastic flow procedure. They are taken as the following values: the dilation angle is 35°; the eccentricity is 0.1; the f_{b0}/f_{c0} is 1.16; the K_c is 0.67 and the viscosity parameter is 0.0001 [21,23,24]. For the pure bending FE model, the constraint effect of steel tubes on

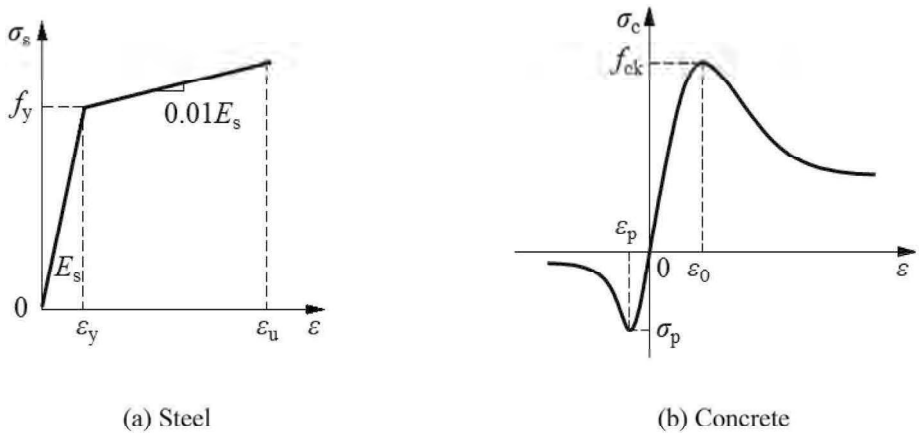

Fig. 3. Uniaxial stress-strain curves of steel and concrete.

concrete is not considered and the input uniaxial stress-strain relationship curve (Fig. 3(b)) of plain concrete is determined according to Appendix C of a China Code for design of concrete structures (GB 50010–2010) [28], as shown below. The d_c and d_t are the damage variable of concrete under uniaxial compression and tensile [28], which characterize the degradation of the elastic stiffness.

(1) Uniaxial compressive stress-strain relationship of concrete

$$\sigma = (1-d_c)E_c\varepsilon \tag{1}$$

$$d_c = \begin{cases} 1-\dfrac{\rho_c n}{n-1+x^n} & (x \le 1) \\ 1-\dfrac{\rho_c n}{\alpha_c(x-1)^2+x} & (x > 1) \end{cases} \tag{2}$$

where $x = \varepsilon/\varepsilon_{c0}$; $\rho_c = f_{ck}/(E_c\varepsilon_{c0})$; $n = E_c\varepsilon_{c0}/(E_c\varepsilon_{c0}-f_{ck})$; $\alpha_c = 0.157 f_{ck}^{0.785}-0.905$; ε_{c0} is peak compressive strain; f_{ck} is prismatic compressive strength; E_c is elastic modulus of concrete.

(2) Uniaxial tension stress-strain relationship of concrete

$$\sigma = (1-d_t)E_c\varepsilon \tag{3}$$

$$d_t = \begin{cases} 1-\rho_t\,1.2-0.2x^5 & (x \le 1) \\ 1-\dfrac{\rho_t}{\alpha_t(x-1)^{1.7}+x} & (x > 1) \end{cases} \tag{4}$$

where $x = \varepsilon/\varepsilon_{t0}$; $\rho_t = f_{tk}/(E_c\varepsilon_{t0})$; $\alpha_t = 0.312 f_{tk}^2$; ε_{t0} is peak tensilestrain; f_{tk} is prismatic tensile strength; N=mm^2.

For FE models subjected to eccentric compression, the constraint effect of the steel tubes on concrete is considered and the input uniaxial stress-strain relationship curve of confined concrete is determined according to Han et al. [22] and Liu et al. [16].

A shell element with four-node reduction integration (S4R) is adopted for the steel tube. A three-dimensional solid element with eight-node reduction integration (C3D8R) is adopted for core concrete.

2.2. Surface interaction, boundary conditions and loading method

A surface-to-surface contact interaction is applied to describe the interaction between steel tube and concrete, specifying a hard contact property in the normal direction and a friction property in the tangential direction with the friction coefficient of 0.25 [21–23]. This interaction allows separation of the concrete and steel tube after tube's local buckling.

In the FE model, the boundary condition and loading scheme are modeled completely according to those in the experiments (Fig. 4). It is worth noting that eccentric loading is achieved by adjusting the position of the rigid body reference point (RP) on the top of column.

2.3. Verification of FE model

Bending-displacement curves of T-shaped CFST columns are calculated with the FE model and compared with experimental results (Fig. 5). As can be seen, simulated bending-displacement curves are in relatively good agreement with the experimental results, which reveals that the bending FE model is reliable. Besides, the steel plate in the black circle in Fig. 6(b) is so close to the neutral axis that the stress is generally $0.2–0.3f_y$ and the flexural strength of TCW1–3 is only 6% higher than that of TCWT1–1 (Fig. 5(a)). Therefore, the T-shaped CFST columns with the same cross-section type as TCWT1–1 is used to carry out flexural strength parametric analysis in the following. Eccentric load versus mid-span horizontal displacement curves and failure models of special-shaped CFST columns are calculated with the FE models and compared with experimental results (Fig. 7). It can be seen from Fig. 7 that the FE calculation results are in good agreement with the experimental results, which shows that the eccentric compression FE models are reliable.

3. Sectional flexural resistances of special-shaped CFST columns

3.1. Parametric analysis

Based on the established bending FEM of T-shaped CFST columns, the bending model of L-shaped CFST columns is established. Then on the base of these, the influence of parameters such as section size, steel ratio α and material strength (f_y, f_{ck}) on the bending mechanical properties of special-shaped CFST columns in the characteristic direction (Fig. 8(a)-(e)) was analyzed. Where YYSY indicates that the neutral axis is parallel to the flange and the flange is the compression zone; YYSL indicates that the neutral axis is parallel to the flange and the flange is the tension zone; PXFB indicates that the neutral axis is parallel to the web. According to the parametric analysis results, the simplified calculation formulae of the flexural resistance of special-shaped CFST columns in the characteristic direction are proposed. Fig. 8(f)-(g) show the dimensions of cross-section of special-shaped CFST columns. The parameter ranges of special-shaped

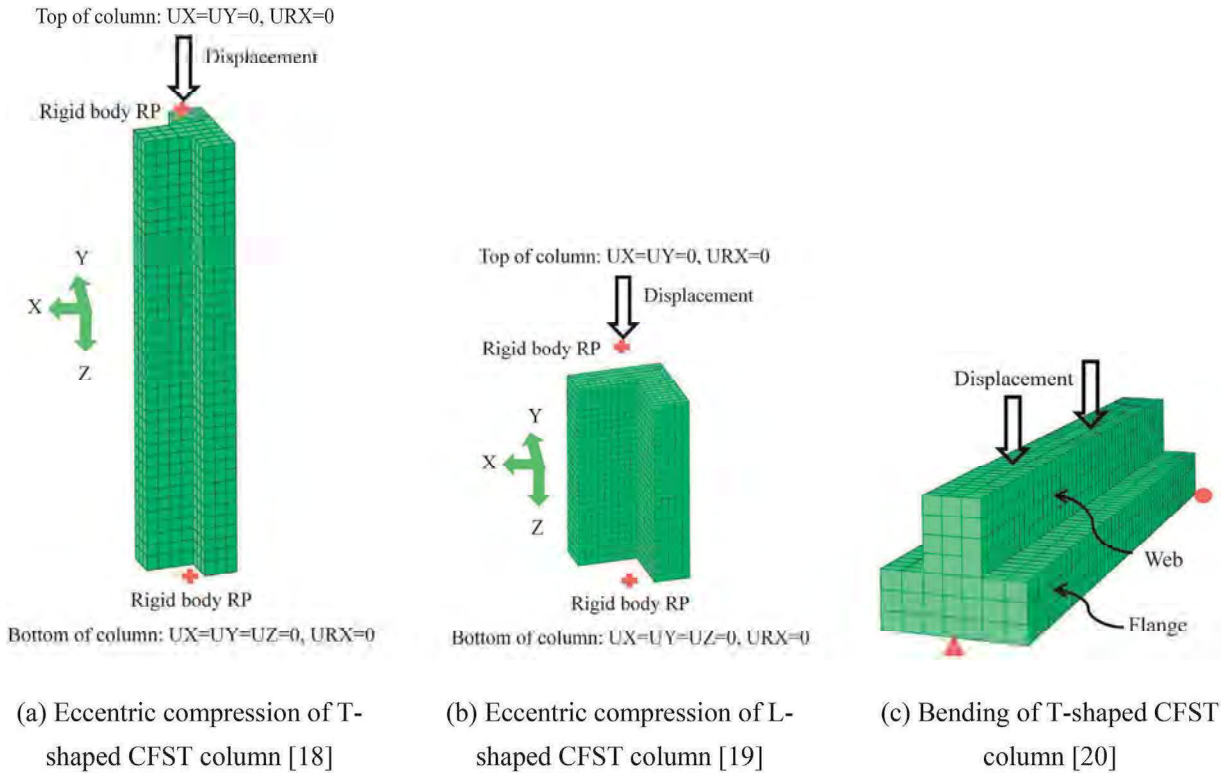

Fig. 4. Boundary conditions and loading schemes of related experimental researches.

CFST columns are as follows: column limb width-to-thickness ratio B/t_w (H/t_w) = 2.0–4.0, thickness of steel tube t = 2.0–4.0 mm, steel-to-concrete ratio α = 3.5%–11.7%, yield strength of steel tube f_y = 235–345 MPa and prismatic compressive strength of concrete f_{ck} = 20.1–40.0 MPa.

Fig. 9 shows the bending moment versus mid-span displacement of special-shaped CFST columns. It can be seen from Fig. 9 that the bending strengths in various characteristic direction are quite different, especially when the cross-sectional size is large. The ultimate bending moment M_u is defined as bending strength when the maximum fiber strain of steel tube in tension zone at mid-span reaches 10,000 $\mu\varepsilon$ [20,29–32]. The parameter analysis results are shown in Table 1 and Table 2.

3.2. Simplified calculation of sectional flexural resistances of special-shaped CFST columns

The following simplified calculation models can be established based on the assumptions: (1) original plane cross-sections remain plane; (2) section plastic stress distribution assumption is applied; (3) the contribution of concrete in tension is neglected; (4) the effect of shear force is omitted; (5) the relative interface slippage of the steel tube and concrete is omitted.

Combining the above assumptions with the stress distribution of the mid-span section calculated by the FEM, the simplified stress distribution model is proposed to derive the formula for calculating the flexural resistance of mid-span section.

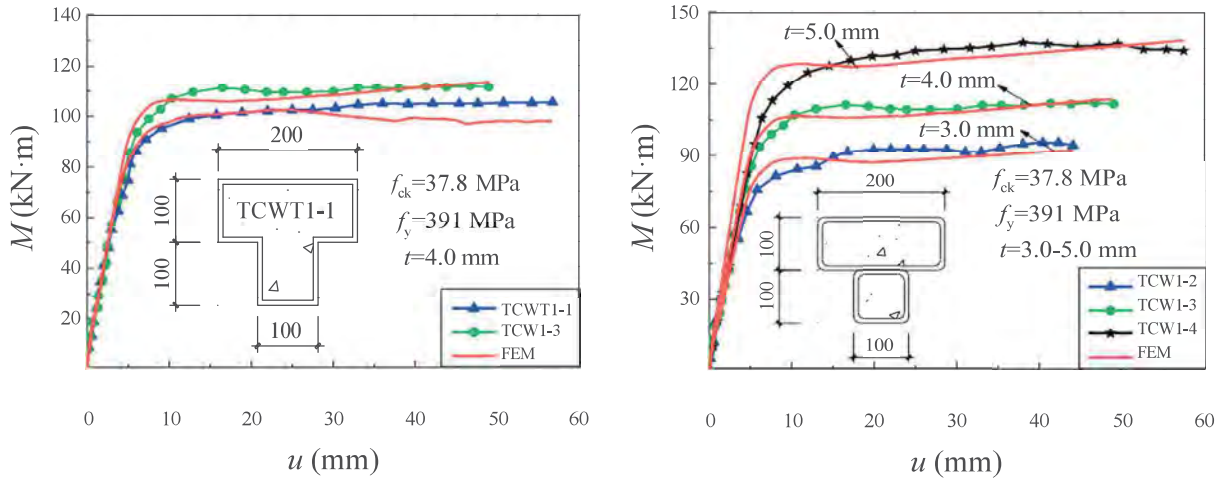

Fig. 5. Comparison of bending-displacement curves between experiment and FEM.

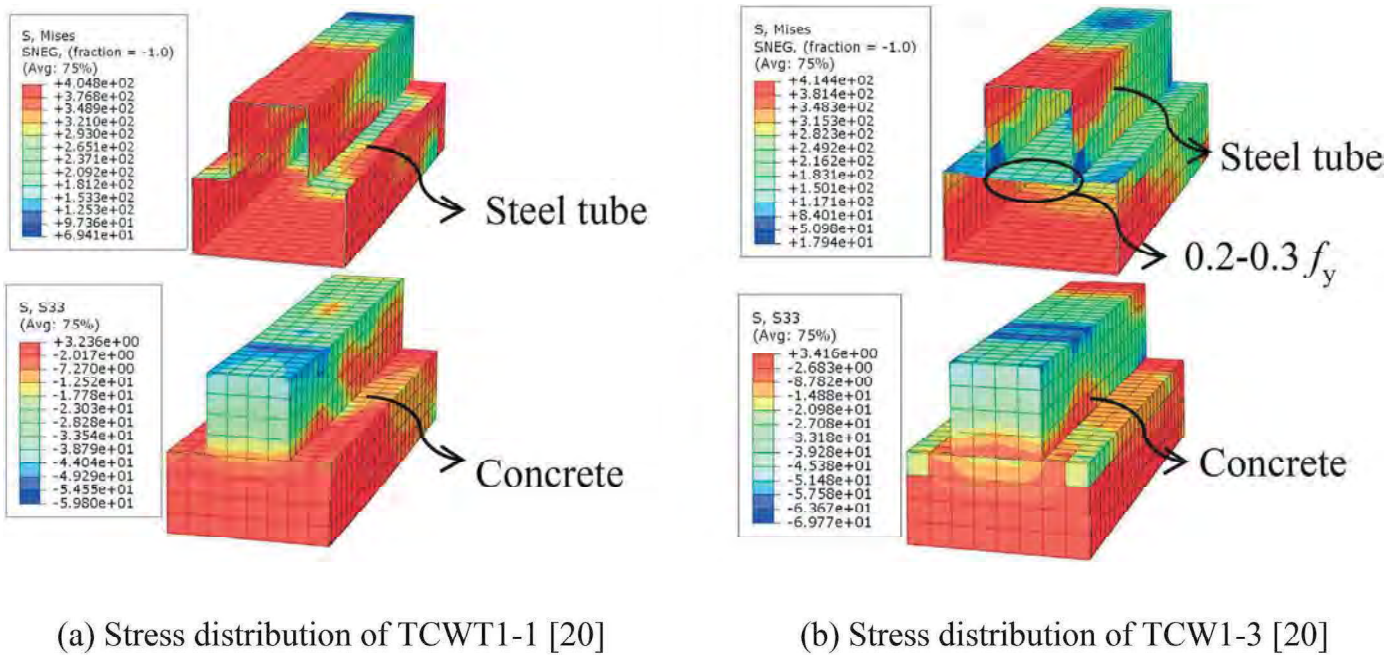

Fig. 6. Stress distribution of TCWT1–1 and TCW1–3 under ultimate state.

3.2.1. The characteristic direction YYSY

1) For the characteristic direction YYSY ($h \le t_w$), the simplified models of the stress distribution of special-shaped CFST columns under ultimate bending moment (cross-sectional plastic bending strength) M_u are shown in Fig. 10. Since the steel plates in the red circle in Fig. 10 (b) and (d) are close to the neutral axis, the stress is generally 0.2–0.35f_y, which contributes little to the bending strength. Therefore, the contribution of the steel plates in the red circle to the bending strength is ignored in simplified calculation.

The calculation formulae for the bending strength of special-shaped CFST columns can be obtained as follows according to the simplified model in Fig. 10.

$$\begin{cases} M_u = Dh^2 + Ph + G \\ h = \dfrac{F}{E} \end{cases} \quad (5)$$

where $E = 4tf_y + (B - 2t)\times f_{ck}$

$F = (B-t_w-2H)tf_y - (B-2t)t \times f_{ck}$

$D = 2tf_y + 0.5(B-2t)f_{ck}$

$P = (B-2H-t_w)tf_y - (B-2t)t \times f_{ck}$

$G = (H-0.5t)t_w tf_y + \left(H^2-2Ht+2t^2\right)tf_y - 0.5Bt^2 f_y + 0.5(B-2t)t^2 f_{ck}$

2) For the characteristic direction YYSY ($h > t_w$), the simplified models of the stress distribution of special-shaped CFST columns under ultimate bending moment M_u are shown in Fig. 11. Since the steel plates in the red circle and the concrete in red rectangle in Fig. 11(b) and (d) are close to the neutral axis, the stress is quite small, which contributes little to the bending strength. Therefore, the contributions of the steel plates in the red circle and the concrete in red rectangle to the bending strength are ignored in simplified calculation.

The calculation formulae for the bending strength of special-shaped CFST columns can be obtained as follows according to the simplified model in Fig. 11.

$$\begin{cases} M_u = Dh^2 + Ph + G \\ h = \dfrac{F}{E} \end{cases} \quad (6)$$

where $E = 4tf_y$

$F = (B-t_w-2H)tf_y + (B-2t)(t_w-2t) \times 1.1f_{ck}$

$D = 2tf_y$

$P = (B-2H-t_w)tf_y + (B-2t)(t_w-2t) \times 1.1f_{ck}$

$G = (H-0.5t)t_w tf_y + \left(H^2-2Ht+2t^2\right)tf_y - 0.5Bt^2 f_y + 0.5(B-2t)(t_w-2t)^2 f_{ck}$

3.2.2. The characteristic direction YYSL

1) For the characteristic direction YYSL ($h \le H\text{-}t_w$), the simplified models of the stress distribution of special-shaped CFST columns under ultimate bending moment M_u are shown in Fig. 12. Since the steel plates in the red circle in Fig. 12(b) and (d) are close to the neutral axis, the stress is generally 0.25–0.40f_y, which contributes little to the bending strength. Therefore, the contribution of the steel plates in the red circle to the bending strength is ignored in simplified calculation.

The calculation formulae for the bending strength of special-shaped CFST columns can be obtained as follows according to the simplified model in Fig. 12.

$$\begin{cases} M_u = Dh^2 + Ph + G \\ h = \dfrac{F}{E} \end{cases} \quad (7)$$

where $E = 4tf_y + (t_w - 2t)\times f_{ck}$

$F = (t_w-B-2H)tf_y - t(t_w-2t) \times f_{ck}$

$D = 2tf_y + 0.5(t_w-2t)f_{ck}$

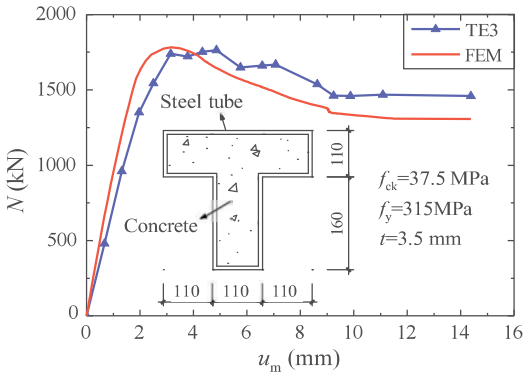

(a) Load versus mid-span horizontal displacement curves of TE2 [18]

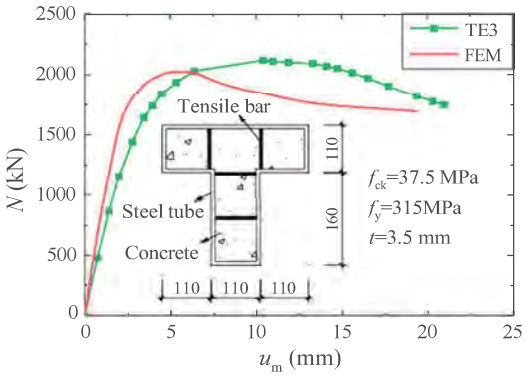

(b) Load versus mid-span horizontal displacement curves of TE3 [18]

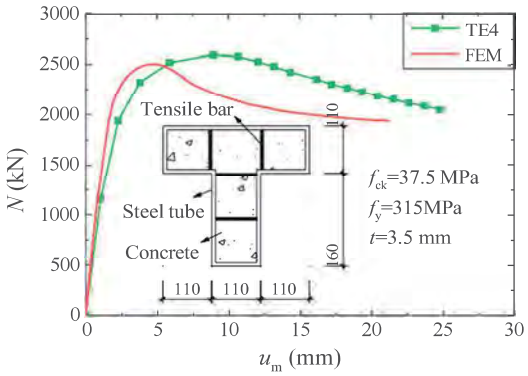

(c) Load versus mid-span horizontal displacement curves of TE4 [18]

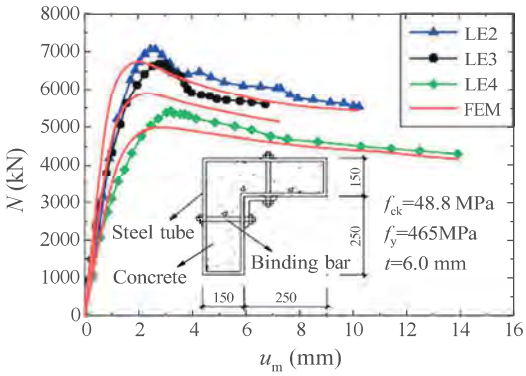

(d) Load versus mid-span horizontal displacement curves of LE2/3/4 [19]

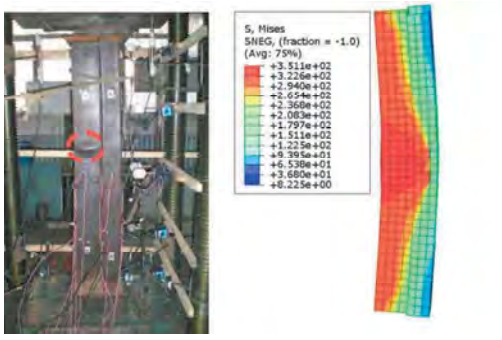

(e) Failure models of TE2 [18]

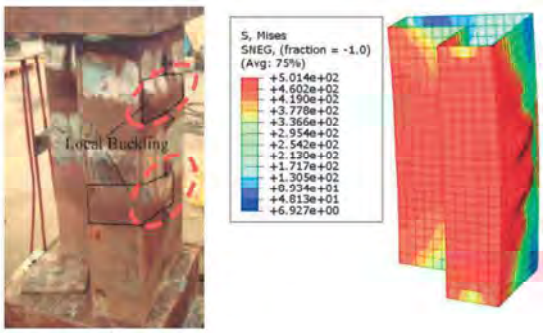

(f) Failure models of LE2 [19]

Fig. 7. Comparison between FEM results and experimental results.

$$P = (t_w - B - 2H + t)f_y - t(t_w - 2t) \times f_{ck}$$

$$G = Btf_y(H - 0.5t) + \left(H^2 - 2Ht + 2t^2\right)tf_y - 0.5t_w t^2 f_y + 0.5(t_w - 2t)t^2 f_{ck}$$

2) For the characteristic direction YYSL (h ~ H-t_w), the simplified models of the stress distribution of special-shaped CFST columns under ultimate bending moment M_u are shown in Fig. 13.

Since the steel plates in the red circle and the concrete in red rectangle in Fig. 13(b) and (d) are close to the neutral axis, the stress is

quite small, which contributes little to the bending strength. There- fore, the contributions of the steel plates in the red circle and the concrete in red rectangle to the bending strength are ignored in sim- plified calculation.

The calculation formulae for the bending strength of special-shaped CFST columns can be obtained as follows according to the simplified model in Fig. 13.

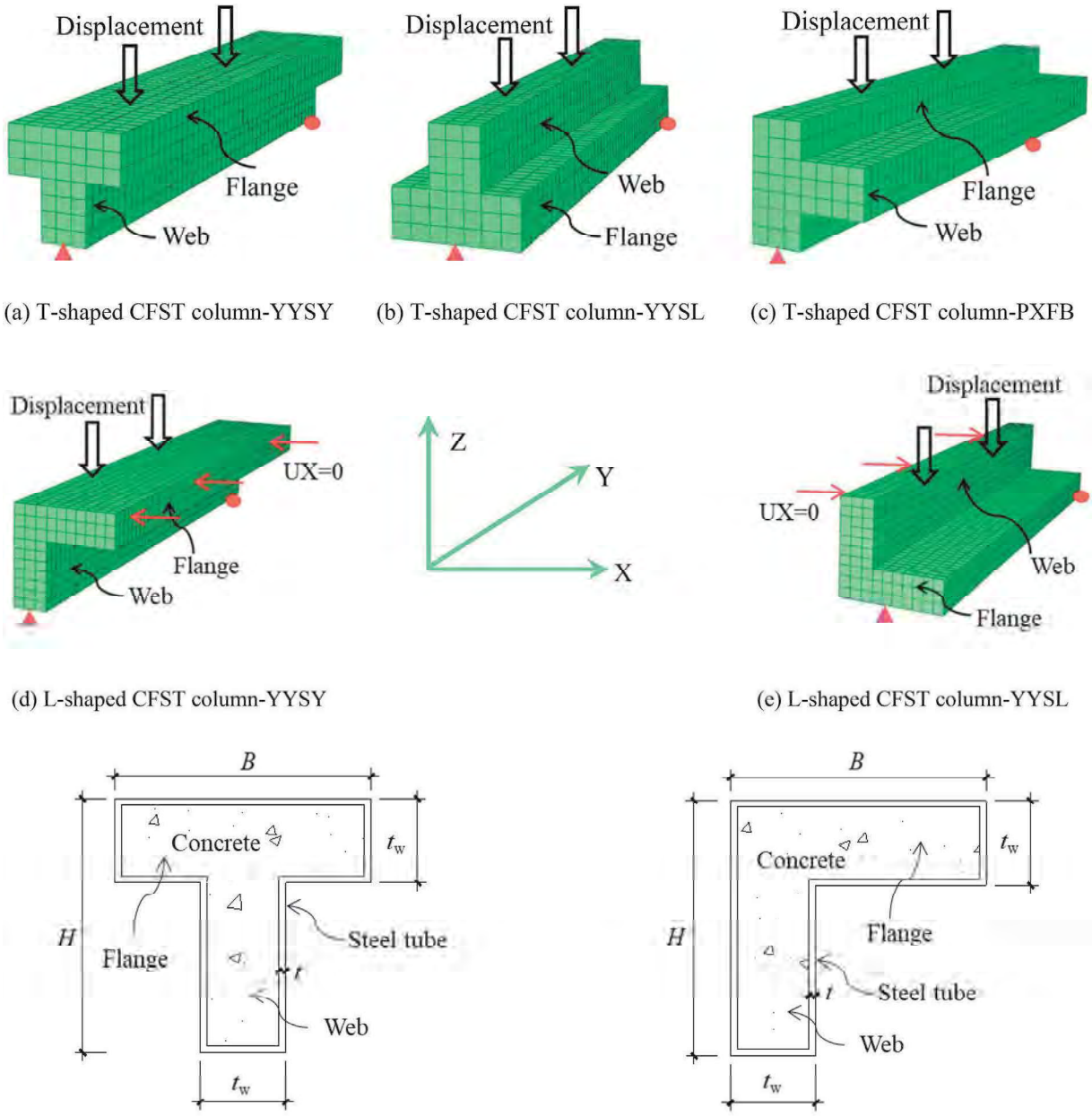

Fig. 8. Bending FEM of special-shaped CFST columns in characteristic direction and cross sections. Note: The symbol "▲" in the figure means the boundary condition is "UX = UY=UZ = 0". The symbol "•" means the boundary condition is "UX = UZ = 0". For the L-shaped column models, the symbol "←" means limiting lateral displacement to avoid torsion.

$$\begin{cases} M_u = Dh^2 + Ph + G \\ h = -\dfrac{F}{E} \end{cases}$$

where $E = 4tf_y$

$$F = (t_w - B - 2H)tf_y + (H - t_w)(t_w - 2t)f_{ck}$$

$$D = 2tf_y$$

$$P = (t_w - B - 2H)tf_y + (t_w - 2t)(H - t_w)f_{ck}$$

$$G = Btf_y(H - 0.5t) + \left(H^2 - 2Ht + 2t^2\right)tf_y - 0.5t_w t^2 f_y + 0.5(t_w - 2t)(H - t_w)^2 f_{ck} \quad (8)$$

3.2.3. The characteristic direction PXFB

1) For the characteristic direction PXFB ($b \le 0.5(B - t_w)$), the simplified models of the stress distribution of special-shaped CFST columns under ultimate bending moment M_u are shown in Fig. 14. Since the steel plates in the red rectangle in Fig. 14(b) and (d) are close to the neutral axis, the stress is generally 0.18–0.27f_y. Therefore, the stress of the steel plates in the red rectangle is approximately assumed to be 0.2f_y in simplified calculation.

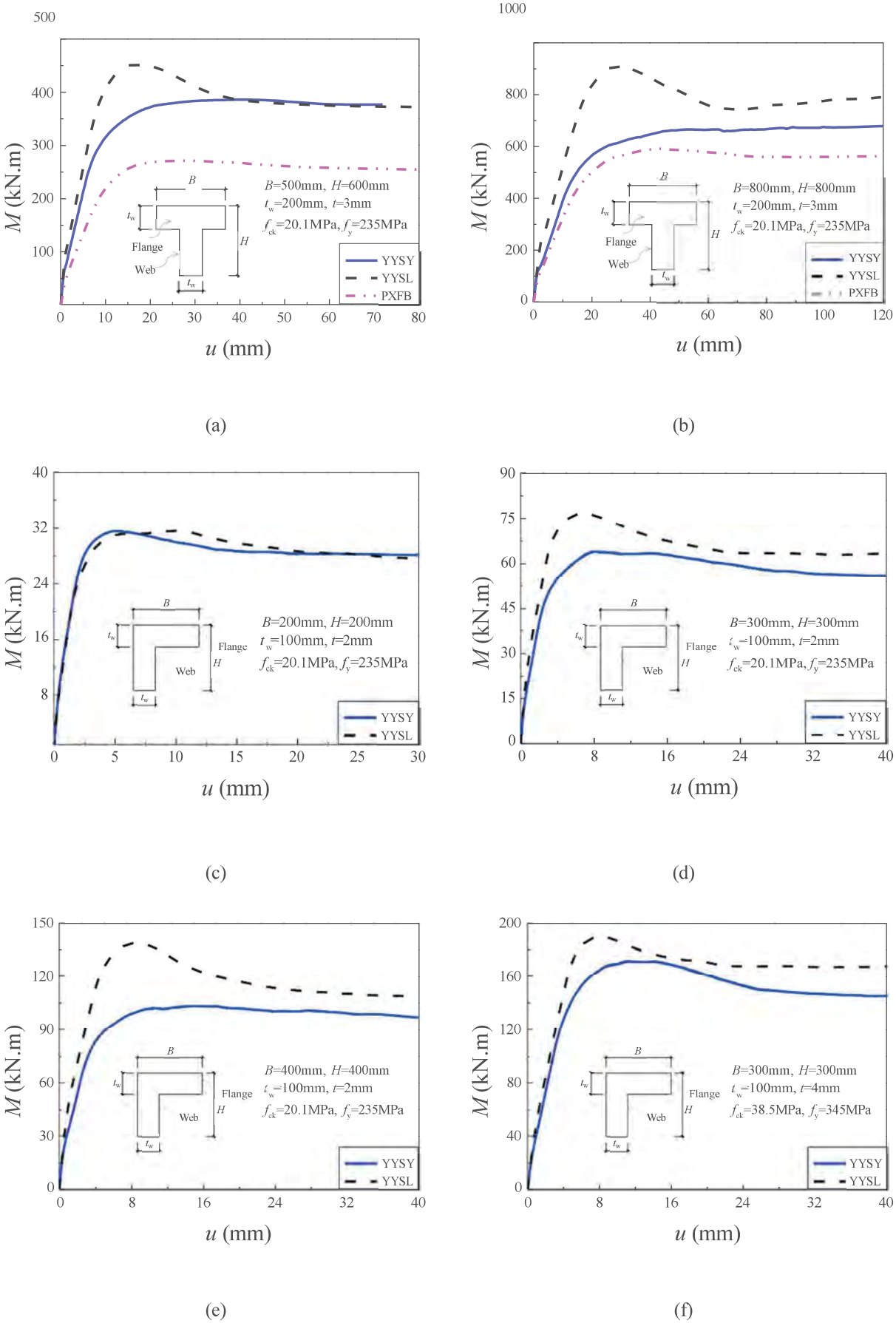

Fig. 9. Bending moment vs. mid-span displacement of special-shaped CFST columns.

Table 1
Parameter analysis results of T-shaped CFST columns.

Dimension of T-shaped section ($B \times H \times t_w$)	Length of column L (mm)	t (mm)	α (%)	f_y (MPa)	f_{ck} (MPa)	M_u (kN·m) (YYSY)	M_u (kN·m) (YYSL)	M_u (kN·m) (PXFB)
200 × 200 × 100	1800	2.0	5.6	235	20.1	31.4	32.8	29.4
200 × 200 × 100	1800	2.0	5.6	345	26.8	45.0	45.9	41.9
200 × 200 × 100	1800	2.0	5.6	345	38.5	47.1	49.1	43.7
200 × 200 × 100	1800	4.0	11.7	235	38.5	63.3	65.0	59.1
200 × 200 × 100	1800	4.0	11.7	345	38.5	87.1	86.5	81.8
300 × 300 × 100	2700	2.0	5.0	235	20.1	65.5	76.8	58.9
300 × 300 × 100	2700	2.0	5.0	345	32.4	94.9	110.9	85.5
300 × 300 × 100	2700	3.0	7.7	235	20.1	90.8	97.2	78.4
300 × 300 × 100	2700	3.0	7.7	345	38.5	115.3	154.5	122.1
300 × 300 × 100	2700	3.0	7.7	235	40.0	99.8	121.6	92.3
300 × 300 × 100	2700	4.0	10.5	345	32.4	173.1	184.7	153.0
300 × 300 × 100	2700	4.0	10.5	345	38.5	179.1	191.3	155.8
400 × 400 × 100	3600	2.0	4.8	235	20.1	106.9	140.2	97.6
400 × 400 × 100	3600	2.0	4.8	235	32.4	107.8	158.4	109.4
400 × 400 × 100	3600	2.0	4.8	235	38.5	115.5	164.6	113.6
400 × 400 × 100	3600	2.0	4.8	345	32.4	150.6	195.0	141.8
400 × 400 × 100	3600	4.0	10.0	345	32.4	283.3	328.8	245.2
500 × 600 × 200	5400	3.0	3.8	235	20.1	385.4	438.2	264.1
600 × 800 × 200	7200	3.0	3.7	235	20.1	644.3	752.0	382.7
800 × 800 × 200	7200	3.0	3.5	235	20.1	664.6	820.3	591.9

Table 2
Parameter analysis results of L-shaped CFST columns.

Dimension of L-shaped section ($B \times H \times t_w$)	Length of column L (mm)	t (mm)	α (%)	f_y (MPa)	f_{ck} (MPa)	M_u (kN·m) (YYSY)	M_u (kN·m) (YYSL)
200 × 200 × 100	1800	2.0	5.6	235	20.1	31.1	31.2
200 × 200 × 100	1800	2.0	5.6	345	26.8	43.4	46.6
200 × 200 × 100	1800	2.0	5.6	345	38.5	44.8	48.8
200 × 200 × 100	1800	4.0	11.7	235	38.5	60.5	63.9
200 × 200 × 100	1800	4.0	11.7	345	38.5	82.0	86.2
300 × 300 × 100	2700	2.0	5.0	235	20.1	64.0	75.4
300 × 300 × 100	2700	2.0	5.0	345	32.4	88.2	107.4
300 × 300 × 100	2700	3.0	7.7	235	20.1	89.2	102.1
300 × 300 × 100	2700	3.0	7.7	345	38.5	131.1	151.2
300 × 300 × 100	2700	4.0	10.5	345	38.5	169.5	187.1
400 × 400 × 100	3600	2.0	4.8	235	20.1	101.9	136.8
400 × 400 × 100	3600	2.0	4.8	235	32.4	108.8	158.6
400 × 400 × 100	3600	2.0	4.8	235	38.5	111.7	164.2
400 × 400 × 100	3600	2.0	4.8	345	32.4	161.8	207.4
400 × 400 × 100	3600	3.0	7.3	345	32.4	214.3	253.1
400 × 400 × 100	3600	4.0	10.0	235	32.4	201.0	255.3

columns under ultimate bending moment M_u are shown in Fig. 15. The stress of the steel plates in the red rectangle in Fig. 15(b) is generally 0.55–0.72f_y. Therefore, the stress of the steel plates in the red rectangle is approximately assumed to be 0.7f_y in simplified calculation.

The calculation formulae for the bending strength of special-shaped CFST columns can be obtained as follows according to the simplified model in Fig. 14.

$$\begin{cases} M_b = Db^2 + Pb + G \\ b = -\dfrac{F}{E} \end{cases} \tag{9}$$

where $E = 4tf_y + (t_w - 2t)f_{ck}$

$F = -(H - t_w)t \times 1.2f_y - t(t_w - 2t)f_{ck}$

$D = 2tf_y + 0.5(t_w - 2t)f_{ck}$

$P = (1.2t_w - 2B - 1.2H + t)f_y - (t_w - 2t)tf_{ck}$

$G = \left(B^2 - 2Bt + 2t^2\right)tf_y + t_w(B - 0.5t + t)f_y$

The calculation formulae for the bending strength of special-shaped CFST columns can be obtained as follows according to the simplified model in Fig. 15.

$$\begin{cases} M_b = Db^2 + Pb + G \\ b = -\dfrac{F}{E} \end{cases} \tag{10}$$

where $E = 4tf_y + 0.5(H - 2t)f_{ck}$

$F = 0.5(B - t_w)(t_w - 2t)f_{ck} + 0.25(H - 2t) \times (t_w - B - 2t)f_{ck} - 2Btf_y - 0.3tf_y(H - t_w + t)$

$D = 2tf_y + 0.25(H - 2t)f_{ck}$

$P = 0.5(B - t_w)(t_w - 2t)f_{ck} - 2Btf_y - 0.25(H - 2t)(B - t_w)f_{ck} + 0.2(H - t_w + t)f_y$

$$\begin{aligned}&\text{þ } 0{:}5\eth H-t_{\mathrm{w}}\text{Þ}\eth 1{:}2B\text{ þ }0{:}8t_{\mathrm{w}}\ -0{:}8t\text{Þ}tf_{\mathrm{y}}\\&\text{þ }0{:}5\eth t_{\mathrm{w}}-2t\text{Þ}t^{2}f_{\mathrm{ck}}-0{:}5t_{\mathrm{w}}t^{2}f_{\mathrm{y}}\end{aligned}$$

2) For the characteristic direction PXFB (b N $0.5(B-t_{\mathrm{w}})$), the simplified models of the stress distribution of special-shaped CFST

$$\begin{aligned}G\text{ ¼ }&\left(B^{2}-2Bt\text{ þ }2t^{2}\ tf_{\mathrm{y}}\text{ þ }Bt\ tf_{\mathrm{w}}\ -t\ t^{2}f_{\mathrm{y}}\text{ þ }\eth H-t\text{ Þ}\right.\\&\eth 0{:}15B\text{ þ }0{:}85t_{\mathrm{w}}-0{:}85t\text{Þ}tf_{\mathrm{y}}\text{ þ }\frac{1}{16}\eth H-2t\text{Þ}\eth B-t_{\mathrm{w}}\text{Þ}^{2}f_{\mathrm{ck}}\\&-\frac{1}{8}\eth t_{\mathrm{w}}-2t\text{Þ}\eth B-t_{\mathrm{w}}\text{Þ}^{2}f_{\mathrm{ck}}\end{aligned}$$

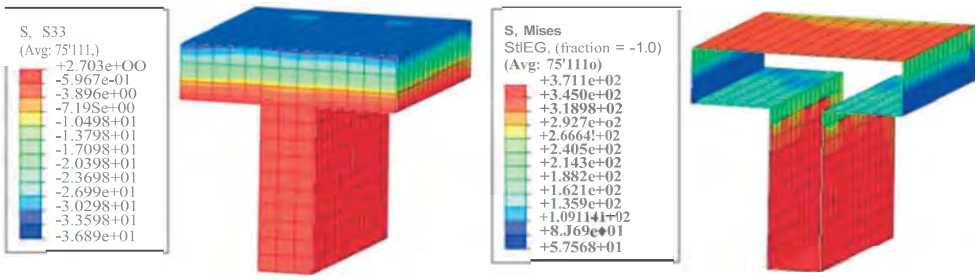

(a) Stress distribution ofT-section (YYSY)

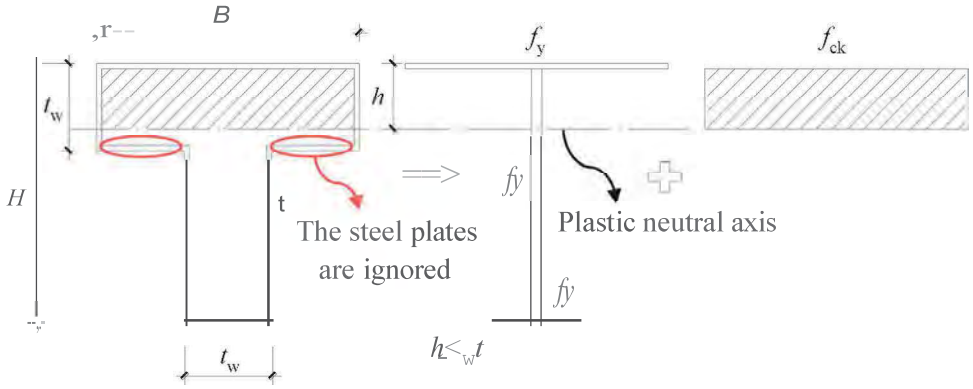

(b) Simplified model of T-section (YYSY)

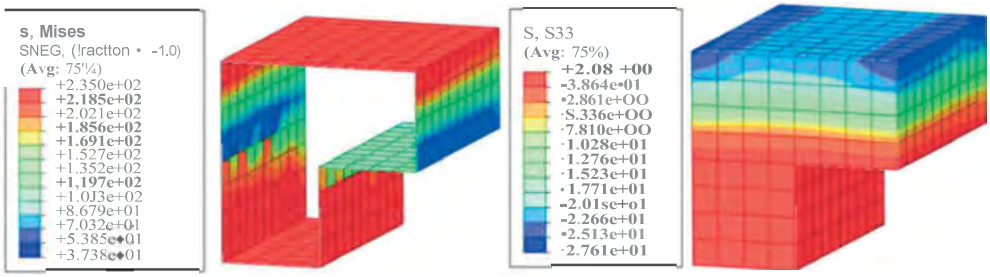

(c) Stress distribution ofL-section **(YYSY)**

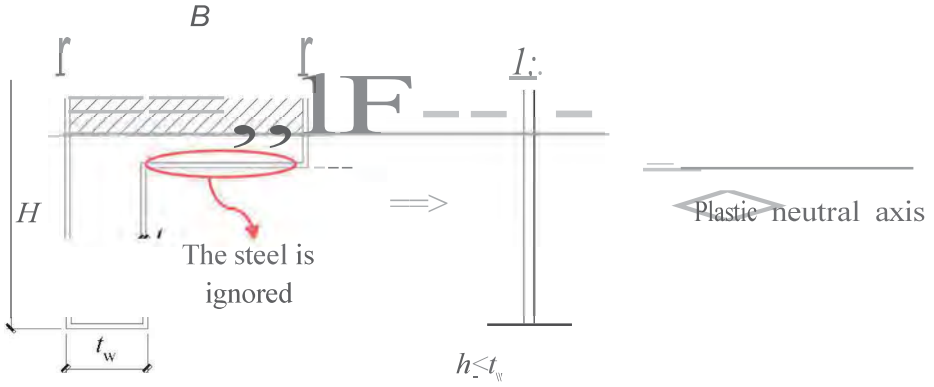

(d) Simplified model ofL-section **(YYSY)**

Fig. 10. Simplified model of special-shaped CFST columns under pure bending (YYSY).

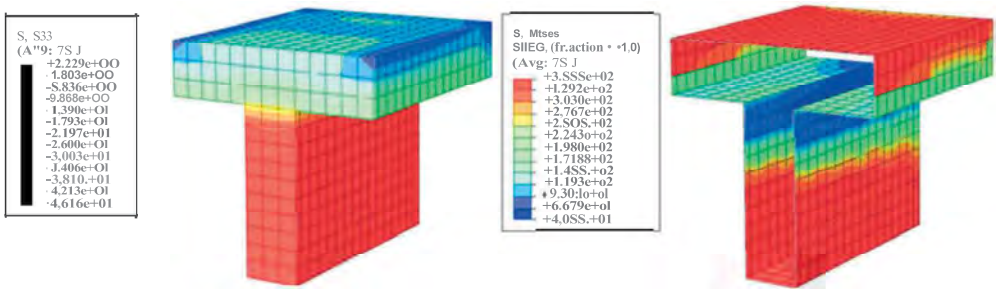

(a) Stress distribution ofT-section (YYSY)

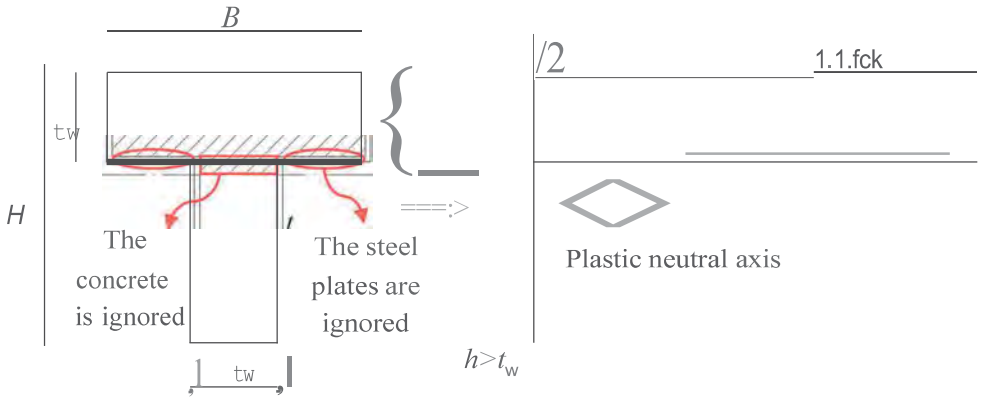

(b) Simplified model ofT-section **(YYSY)**

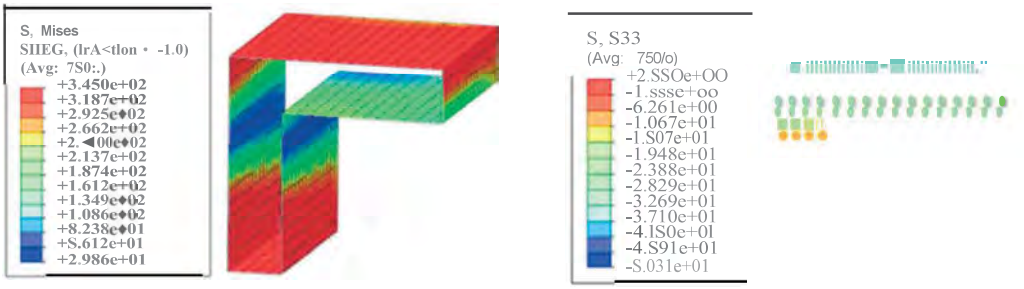

(c) Stress distribution ofL-section (YYSY)

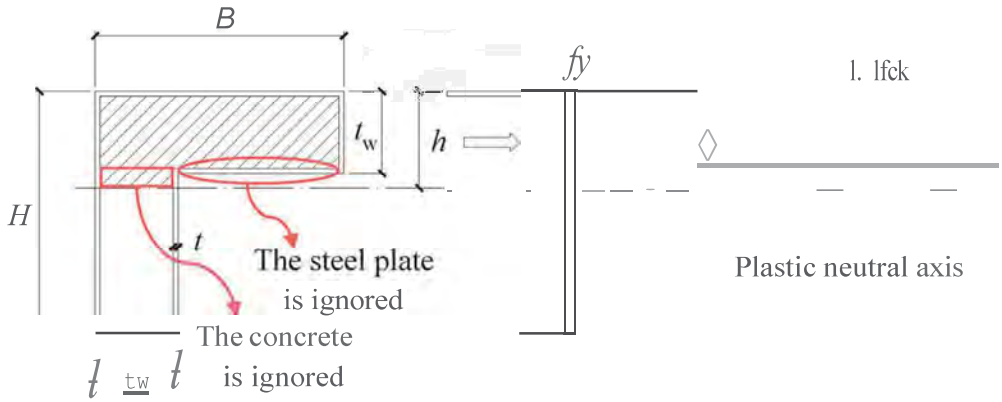

(d) Simplified model ofL-section (YYSY)

Fig. 11. Simplified model of stress distribution of special-shaped CFST columns under pure bending (YYSY).

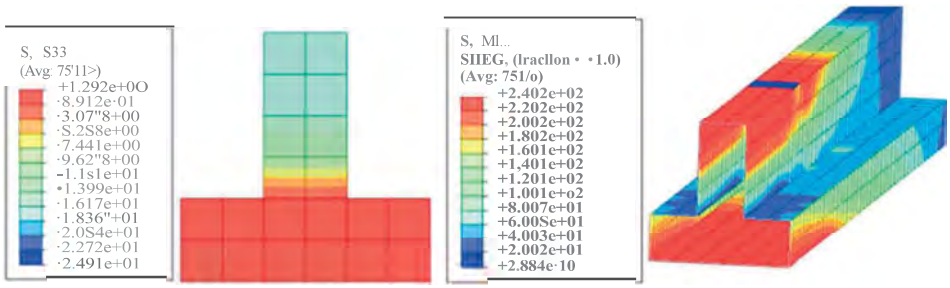

(a) Stress distribution of T-section (YYSL)

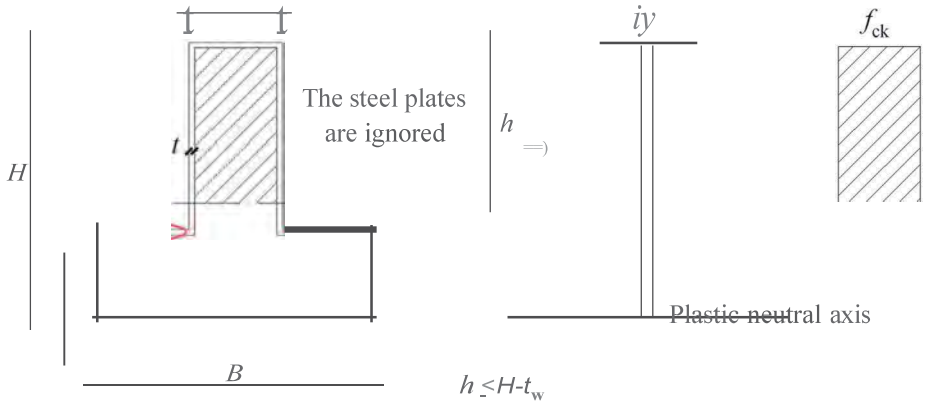

(b) Simplified model of stress distribution (YYSL)

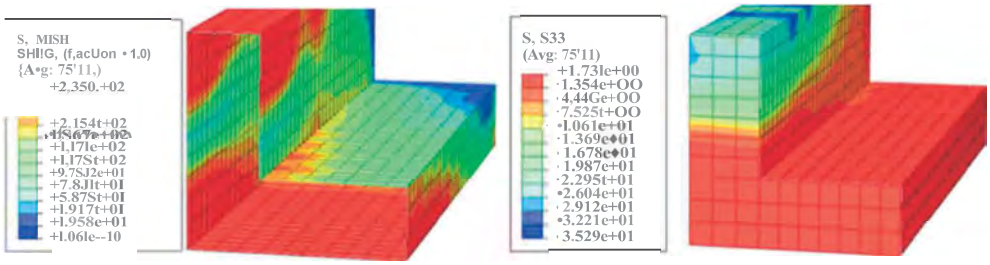

(c) Stress distribution ofL-section (YYSL)

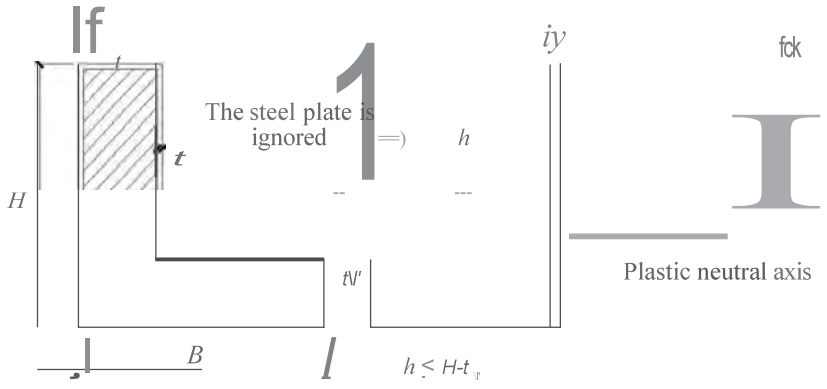

(d) Simplified model of stress distribution (YYSL)

Fig. 12. Simplified model of stress distribution of special-shaped CFST columns under pure bending (YYSL).

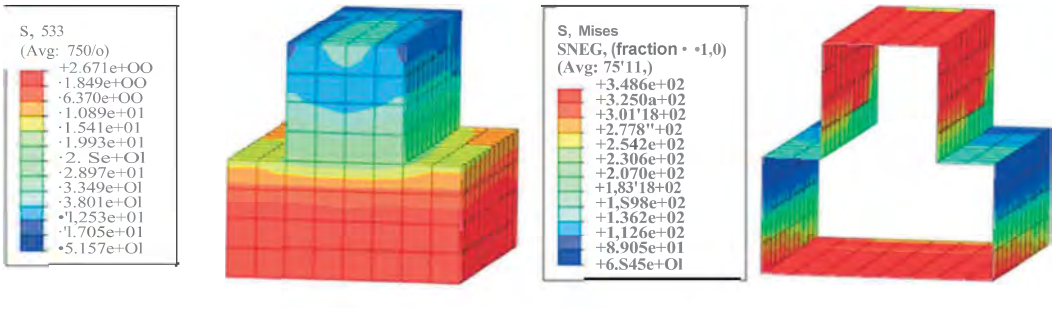

(a) Stress distribution of T-section (YYSL)

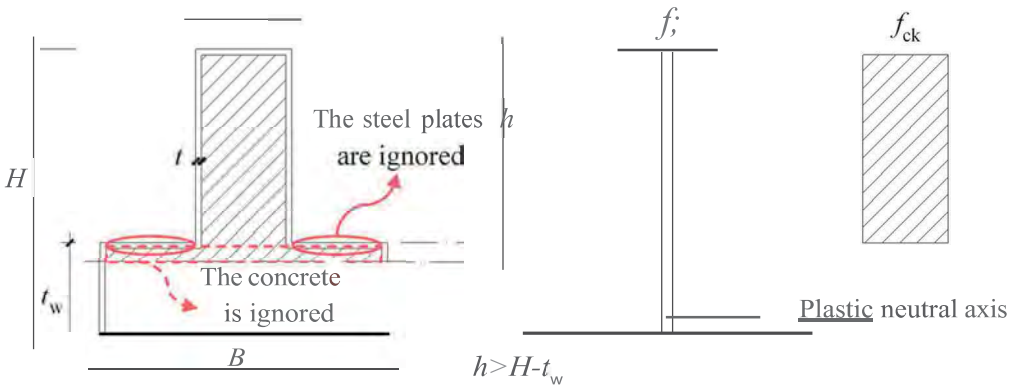

(b) Simplified model of stress distribution (YYSL)

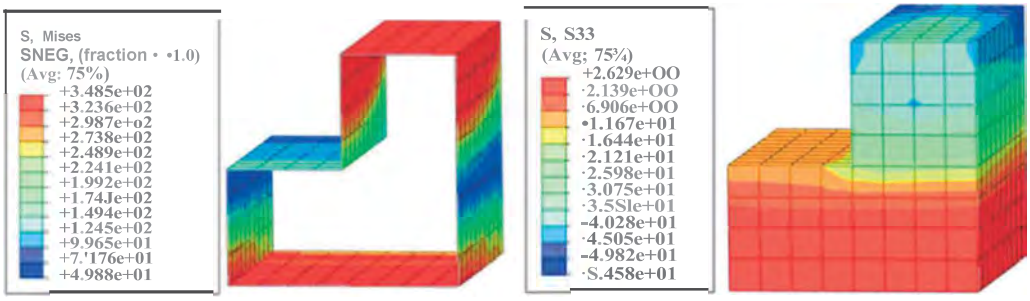

(c) Stress distribution of L-section (YYSL)

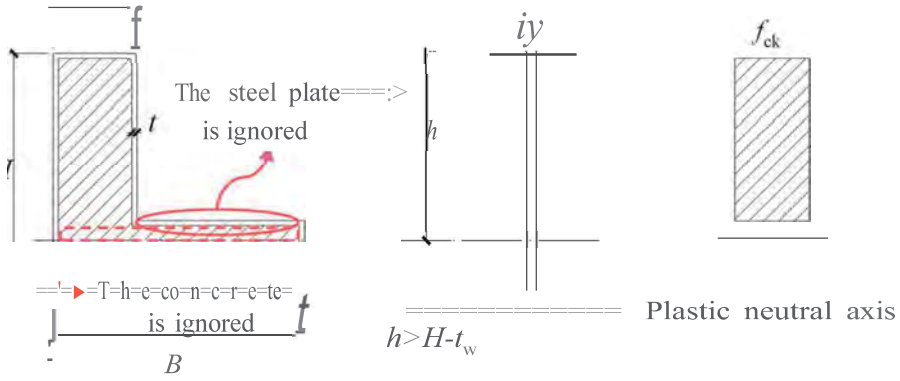

(d) Simplified model of stress distribution (YYSL)

Fig. 13. Simplified model of stress distribution of special-shaped CFST columns under pure bending (YYSL).

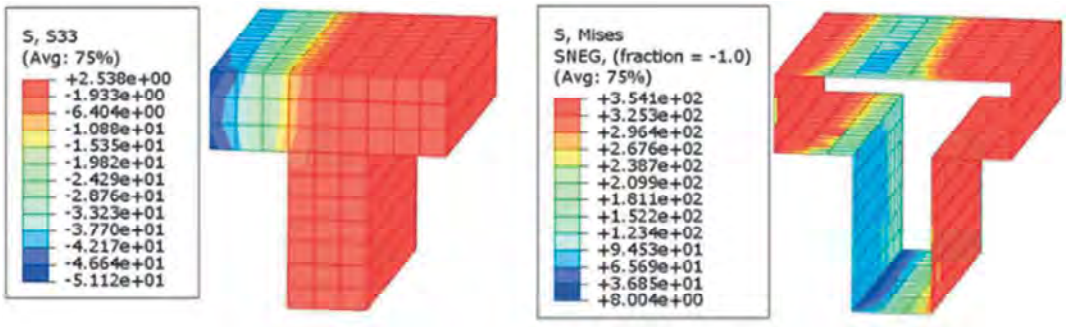

(a) Stress distribution of T-section (PXFB)

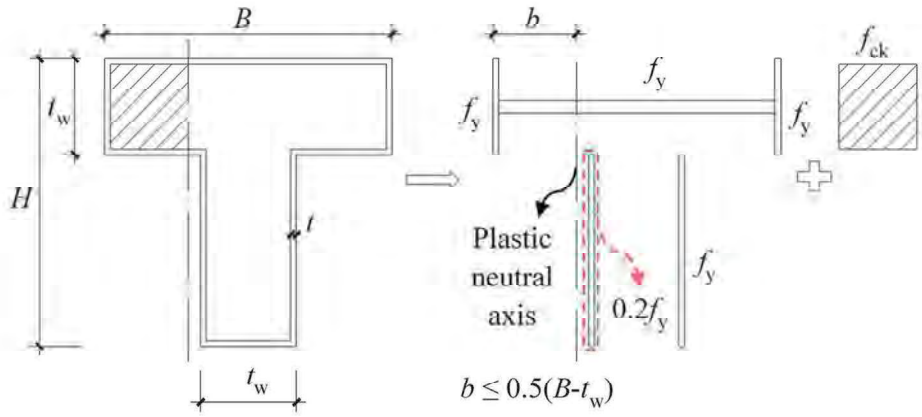

(b) Simplified model of stress distribution (PXFB)

Fig. 14. Simplified model of stress distribution of special-shaped CFST columns under pure bending (YYSL).

3.3. Comparison of sectional flexural resistances between FEM calculations and the simplified calculations

Table 3 is the comparisons of sectional flexural resistance of special-shaped CFST columns between FEM calculations and the simplified model calculations, where $M_{u,FEM}$ is the FEM calculation value; M_{u1} is the calculated value according to the simplified formulae in this paper. As can be seen from Table 3, $M_{u1}/M_{u,FEM}$ of T-shaped CFST columns in different characteristic directions are respectively 0.83 (YYSY), 0.87 (YYSL) and 0.97 (PXFB). And $M_{u1}/M_{u,FEM}$ of L-shaped CFST columns in different characteristic directions are respectively 0.89 (YYSY) and 0.88 (YYSL). Therefore, the simplified calculation formulae proposed in this paper can slightly conservatively predict the sectional flexural resistance of special-shaped CFST columns in different characteristic directions.

4. Resistances of special-shaped CFST columns subjected to eccentric compression

Fig. 16 is a schematic diagram of special-shaped CFST columns under eccentric compressive loads. In the diagram, e represents the eccentricity; N represents the eccentric load. For the T-shaped and L-shaped section with equal limb in flange and web ($B = H$), the range of loading angle ϑ from $-90°$ to 90°should be studied due to the symmetry of the sections. For uniaxial eccentric compression of T-shaped CFST column (Fig. 16(a)), the neutral axis parallels the web when the loading angle ϑ is 0°, that is the characteristic direction PXFB; the neutral axis parallels the flange and the flange is the tension zone when the loading angle ϑ is 90°, that is the characteristic direction YYSL; the neutral axis parallels the flange and the flange is the compression zone when the loading angle ϑ is $-90°$, that is the characteristic direction YYSY. For uniaxial eccentric compression of L-shaped CFST column (Fig. 16(b)), the neutral axis parallels the flange and the flange is the tension zone when the loading angle ϑ is 135° (45°), that is the characteristic direction YYSL; the neutral axis is parallels the flange and the flange is the compression zone when the loading angle ϑ is $-45°$ ($-135°$), that is the characteristic direction YYSY. When the loading angle ϑ is not the values above, the sections are considered under biaxial eccentric compression.

4.1. Uniaxial eccentric compression

4.1.1. Parametric analysis

The dimensions of cross-section of special-shaped CFST columns are shown Fig. 8. A total of 672 special-shaped CFST stub columns subjected to eccentric compression are analyzed. Some typical results can be seen from Fig. 17, in which the section sizes (B, H, t_w), the steel ratio (α), the concrete strength grade (f_{ck}), the steel strength grade (f_y) and the loading angle (ϑ) have significant influences on the N-M curves, and the convex portion of the N-M curves has a certain symmetry. The parameter ranges of special-shaped CFST columns subjected to eccentric compression are same as those under pure bending in section 3.

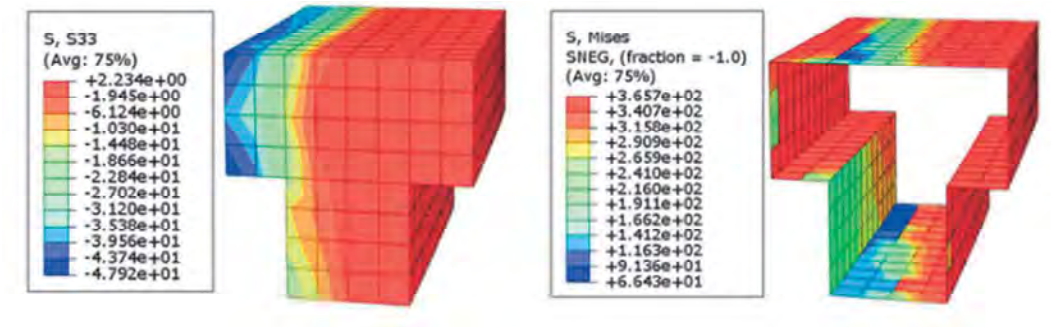

(a) Stress distribution of T-section (PXFB)

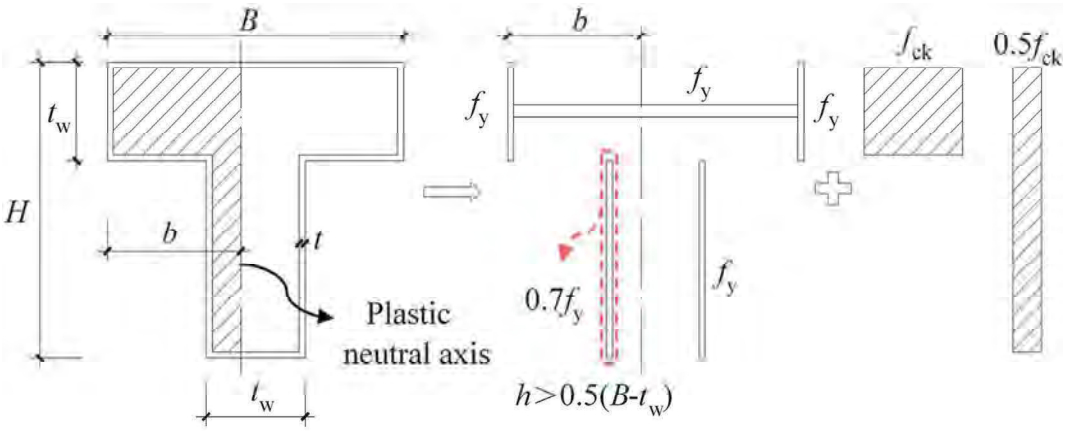

(b) Simplified model of stress distribution (PXFB)

Fig. 15. Simplified model of stress distribution of special-shaped CFST columns under pure bending (YYSL).

Table 3
The comparison of sectional flexural resistance of special-shaped CFST column.

Characteristic direction	T-shaped section ($B \times H \times t_w$)	Steel ratio α (%)	Steel tube f_y (MPa)	Concrete f_{ck} (MPa)	–	$M_{u1}/M_{u,FEM}$
YYSY	200 × 200 × 100	3.5–11.7	235–345	20.1–40.0	Range	0.79–0.90
	300 × 300 × 100				Average value	0.83
	400 × 400 × 100				Standard deviation	0.027
YYSL	500 × 600 × 200				Range	0.77–0.94
	600 × 800 × 200				Average value	0.87
	800 × 800 × 200				Standard deviation	0.051
PXFB					Range	0.66–0.86
					Average value	0.78
					Standard deviation	0.049
Characteristic direction	L-shaped section ($B \times H \times t_w$)	Steel ratio α (%)	Steel tube f_y (MPa)	Concrete f_{ck} (MPa)	–	$M_{u1}/M_{u,FEM}$
YYSY	200 × 200 × 100	4.8–11.7	235–345	20.1–40.0	Range	0.83–0.94
	300 × 300 × 100				Average value	0.89
	400 × 400 × 100				Standard deviation	0.032
YYSL					Range	0.76–0.95
					Average value	0.88
					Standard deviation	0.057

B× H× t_w is the T-shaped and L-shaped cross-sectional dimensions (in Fig. 8(f) and (g)). α is the area ratio of steel to concrete. f_{ck} is the concrete prismatic compressive strength. f_y is the steel yield strength. $M_{u,FEM}$ is the FEM calculation value. M_{u1} is the calculated value according to Eq. (5)-(10) in this paper. $N_{c,FEM}$ and $M_{c,FEM}$ are the FEM calculation values. N_{c1} and M_{c1} are the calculated values according to the Eq. (12)-(14) in this paper.

4.1.2. Simplified calculation of cross-sectional N-M interaction curves

According to the parametric analysis results, it can be summarized that the *N-M* interaction curve of special-shaped CFST columns can be simplified into three straight lines, as shown by the red dotted line in Fig. 18(a). Accordingly, the calculation formulae of the simplified curve are shown in Eq. (11). The point A repre- sents the sectional axial resistance N_u [16]; the point D represents the pure bending resistance M_u and determined by the simplified calculation formulae in section 3.2 of this paper; the point C represents the point with the maximum bending resistance; the bending resistance of point B is assumed to be the same with point D, ie $M_b = M_u$. It can be seen from the parametric analysis that the *N-M* interaction curve BCD has a certain symmetry, N_b is approximately equal to $2N_c$ to simplify the calculation. The stress distributions of special-shaped CFST columns corresponding to each characteristic point (D, C, B and A) are shown in Fig. 18 (b) and (c). In summary, this section mainly researches the calculation method of point C.

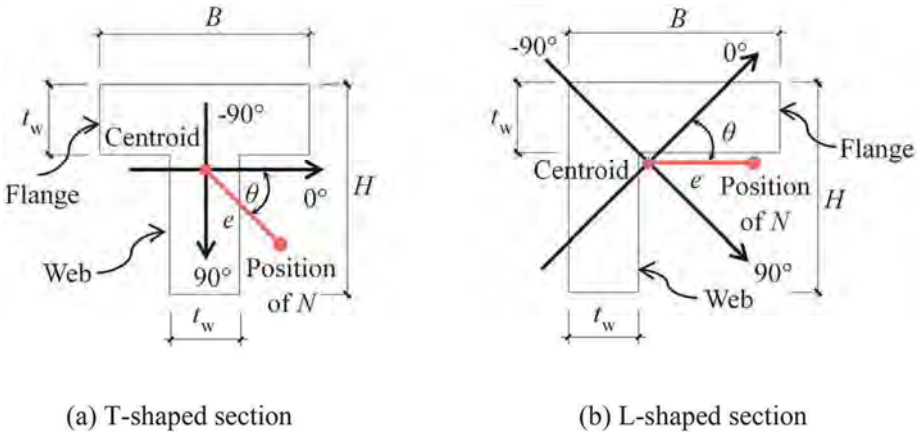

Fig. 16. Schematic diagram of the special-shaped CFST column under eccentric compressive load.

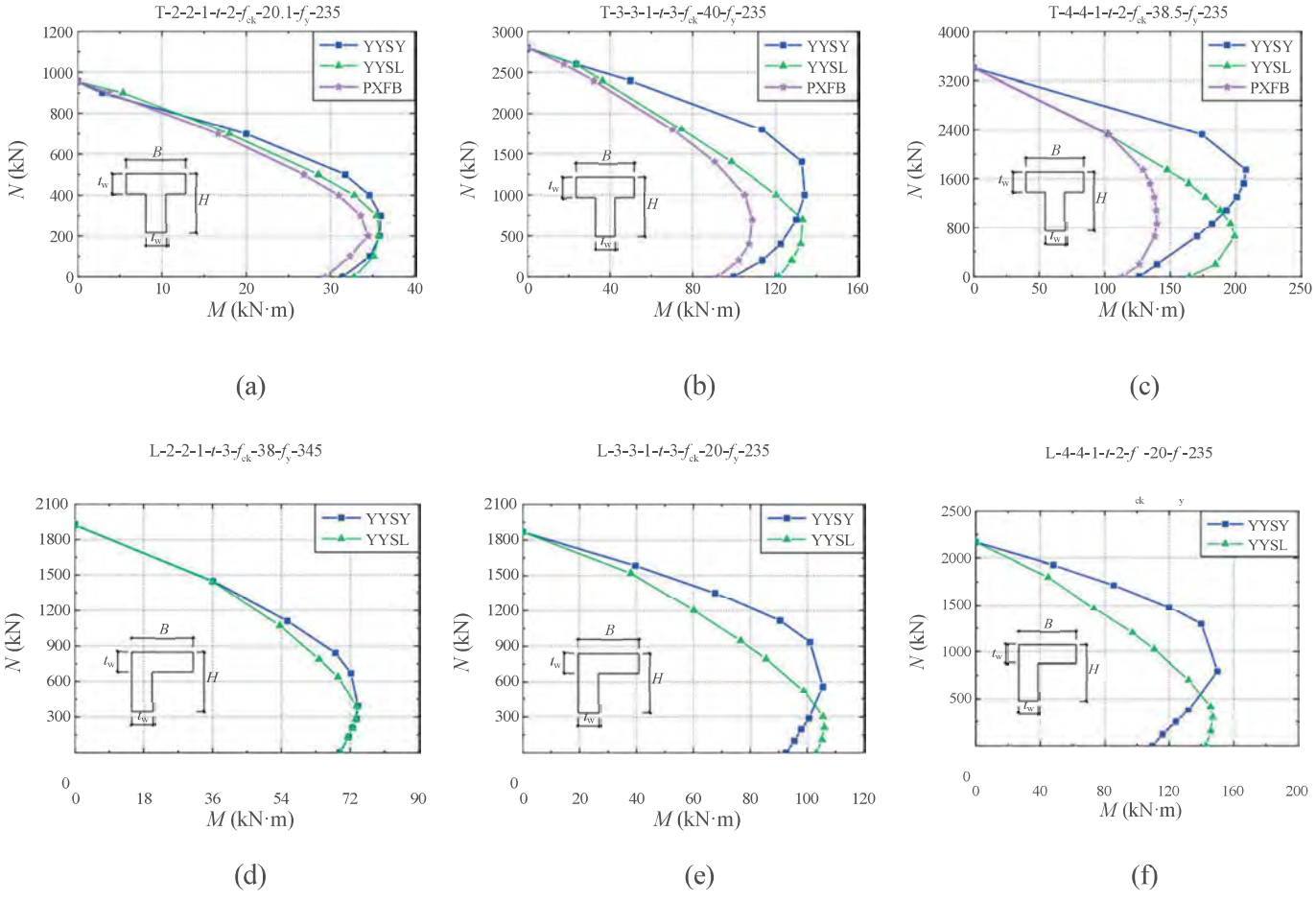

Fig. 17. *N*-*M* curves of special-shaped CFST columns. Note: The naming rule of specimens is, for example, "T-2-2-1-*t*-2-f_{ck}-20.1-f_y-235", "T" means T-section; "2–2-1" means $B = 200$, $H = 200$, $t_w = 100$; "*t*-2" means that the thickness of the steel tube is 2 mm; "f_{ck}-20.1" means that the prismatic compressive strength of concrete is 20.1 MPa; "f_y-235" means that the yield strength of steel tube is 235 MPa.

$$\text{AB}: \quad \frac{N-N_b}{N_u-N_b} + \frac{M}{M_b} \leq 1$$

$$\text{BC}: \quad \frac{N-N_b}{N_c-N_b} + \frac{M-M_c}{M_b-M_c} \leq 1 \qquad (11)$$

$$\text{CD}: \quad \frac{N}{N_c} + \frac{M-M_c}{M_u-M_c} \leq 1$$

Figs. 19–20 that the section plasticity neutral axis position is close to the centroid position. The position of the plastic neutral axis in the section is statistically summarized in Table 4. It can be found that the absolute error between the position of plastic neutral axis and the position of centroidal axis is basically within 5%. Therefore, it is approximated that the neutral axis passes through the sectional

Figs. 19–20 show the cross-sectional stress distributions of T-shaped and L-shaped CFST columns at point C. It can be seen from

4.1.3. The simplified calculation method of point C

centroid when simply calculating the N_c and M_c.

It can be seen from Figs. 19–20 that the steel plate and concrete near the boundary between the flange and the web are so close to the neutral axis that their stress can be neglected when the neutral axis is parallel to the flange (YYSY and YYSL). Therefore, when simply calculating the N_c and M_c, the sectional stress distribution is simplified based on the as- sumptions (see section 3.2 in this paper) and the FEM results, as shown

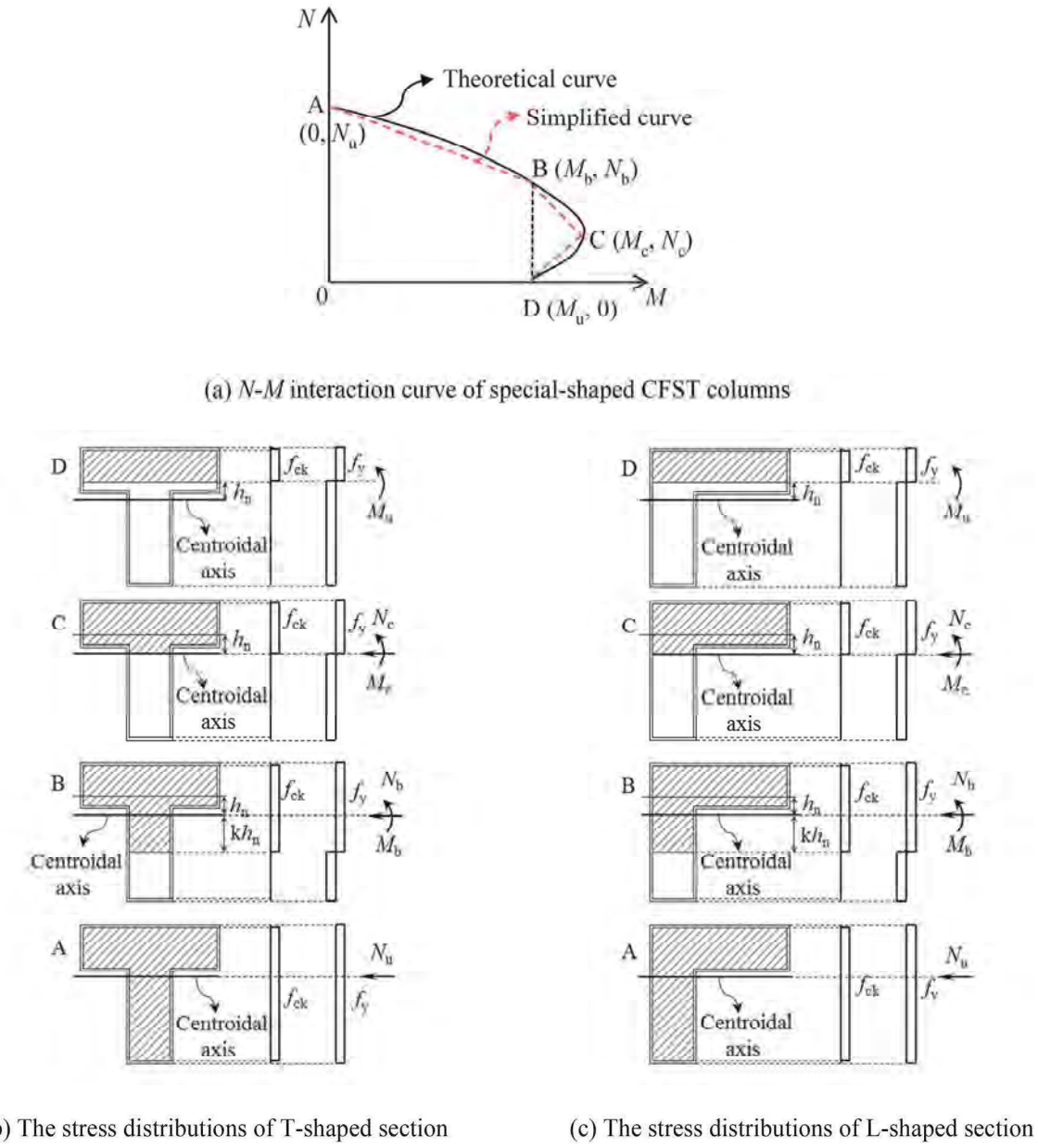

(a) *N-M* interaction curve of special-shaped CFST columns

(b) The stress distributions of T-shaped section

(c) The stress distributions of L-shaped section

Fig. 18. Simplified *N-M* interaction curve and the stress distributions of characteristic point.

in Fig. 21. For YYSY (Fig. 21(a)), the T-shaped and L-shaped steel tube are simplified into an I-shaped steel and all sections are yielding. The stress of concrete in the compression zone is taken as $1.1f_{ck}$ to consider the bending contribution of the neglected part in red rectangle (Fig. 21(a)).

For YYSL (Fig. 21(b)), the T-shaped and L-shaped steel tube are simplified into an I-shaped steel and all sections are yielding. The stress of concrete in the compression zone is taken as f_{ck}. For PXFB, the T-shaped steel tube is simplified and the stresses of steel plates and concrete are shown as Fig. 21(c) based on the Mises distributions (Fig. 19(c)).

(1) For YYSY, the calculation formulae of N_c and M_c can be obtained as follows according to the simplified model of stress distribution in Fig. 21(a).

$$N_c = Eh + F$$
$$M_c = Dh^2 + Ph + G$$

$$F = (B - t_w - 2H)tf_y + (B - 2t)(t_w - 2t) \times 1.1f_{ck}$$

$$D = 2tf_y$$

$$P = (B - 2H - t_w)tf_y + (B - 2t)(t_w - 2t) \times 1.1f_{ck}$$

$$G = (H - 0.5t)t_w tf_y + \left(H^2 - 2Ht + 2t^2\right)tf_y - 0.5Bt^2 f_y + 0.55(B - 2t)(t_w - 2t)^2 f_{ck}$$

(2) For YYSL, the calculation formulae of N_c and M_c can be obtained as follows according to the simplified model of stress distribution in Fig. 21(b).

$$N_c = Eh + F$$
$$M_c = Dh^2 + Ph + G$$

(13)

where $E = 4tf_{y}$

where $E = 4tf_{y} + (t_{w} - 2t) \times f_{ck}$

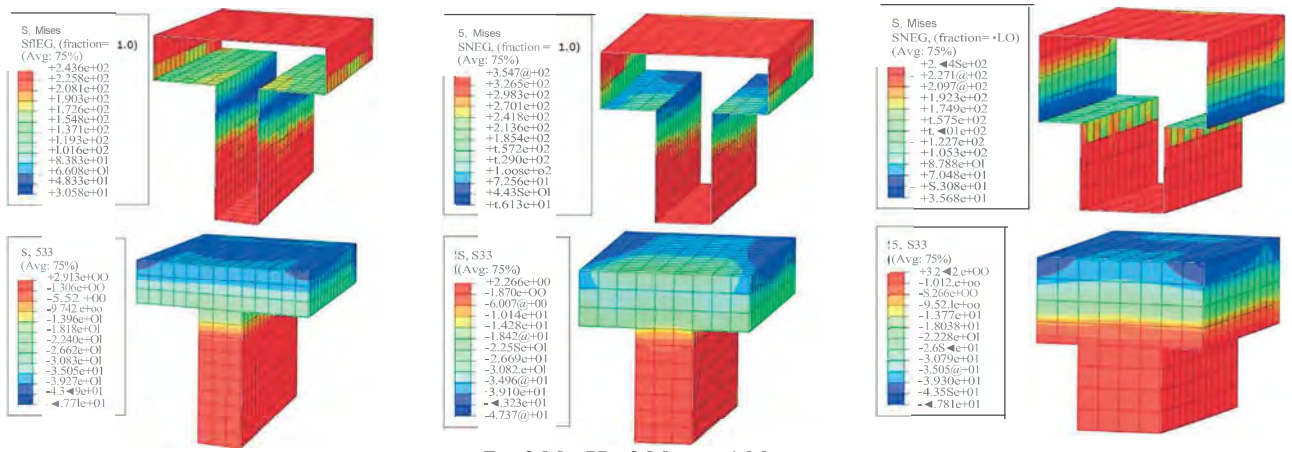

B=400, H=400, tw=100 *B=300, H=300, tw=100* *B=200, H=200, tw=100*

(a) **YYSY**

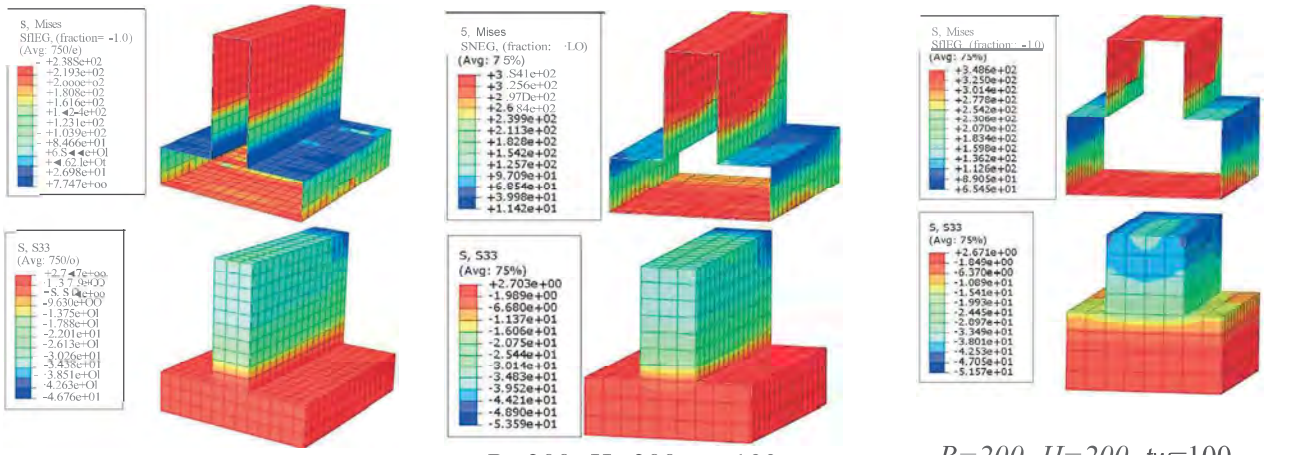

B=400, H=400, tw=100 *B=300, H=300, tw=100* *B=200, H=200, tw=100*

(b) YYSL

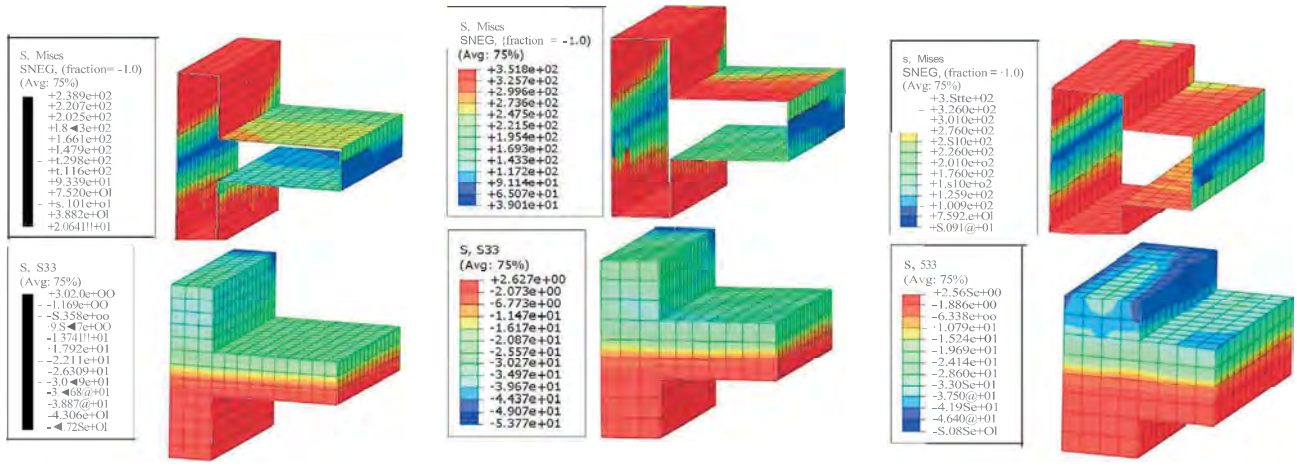

B=400, H=400, tw=100 *B=300, H=300, tw=100* *B=200, H=200, tw=100*

(c) **PXFB**

Fig. 19. Stress distributions of T-shaped CFST columns at point C.

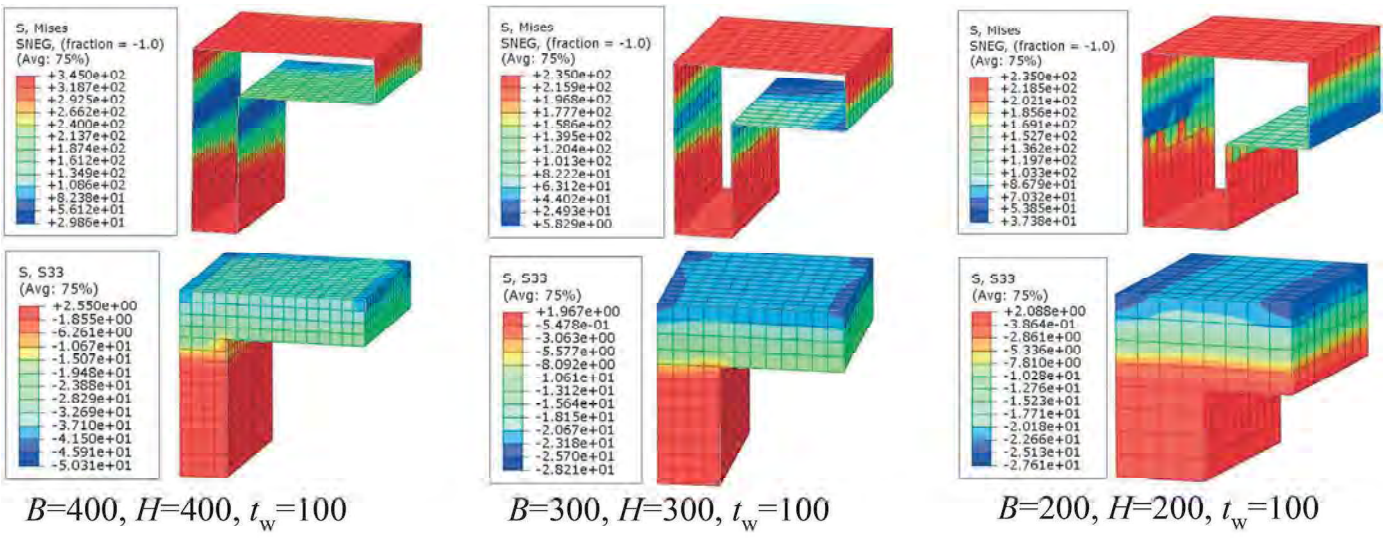

(a) YYSY

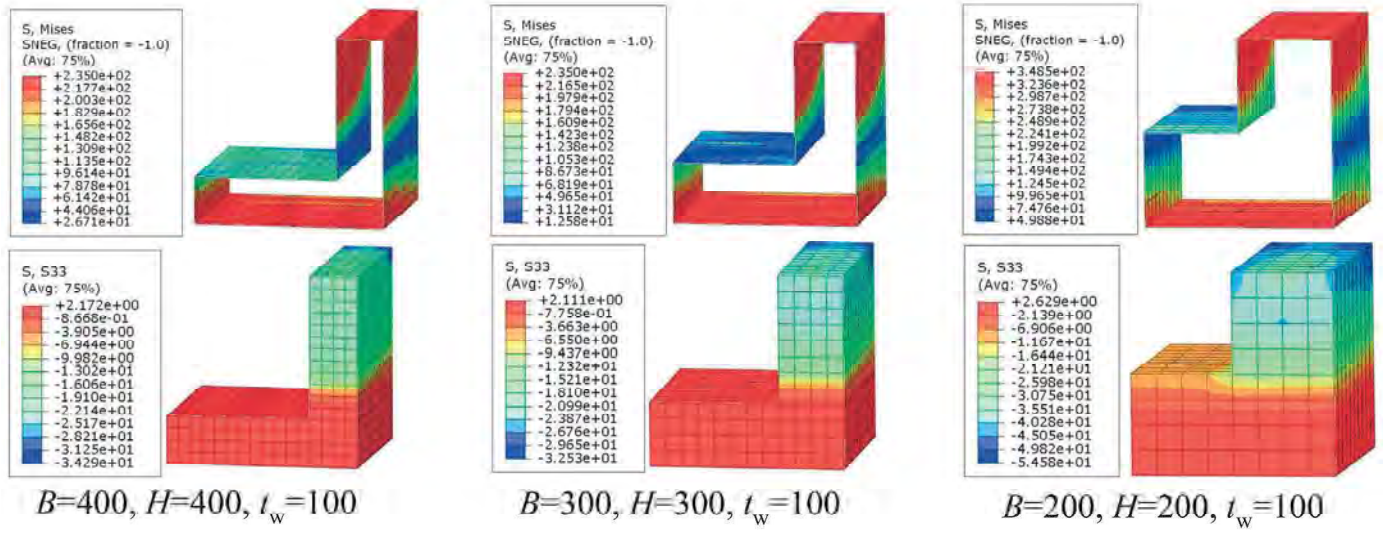

(b) YYSL

Fig. 20. Stress distributions of L-shaped CFST columns at point C.

$$F = (t_w - B - 2H)tf_y - t(t_w - 2t) \times f_{ck}$$

$$D = 2tf_y + 0.5(t_w - 2t)f_{ck}$$

$$P = (t_w - B - 2H)tf_y - t(t_w - 2t) \times f_{ck}$$

$$G = Btf_y(H - 0.5t) + \left(H^2 - 2Ht + 2t^2\right)tf_y - 0.5t_w t^2 f_y + 0.5(t_w - 2t)t^2 f_{ck}.$$

(3) For PXFB, the calculation formulae of N_c and M_c can be obtained as follows according to the simplified model of stress distribution in Fig. 21(c).

$$\begin{cases} N_c = Eb + F \\ M_c = Db^2 + Pb + G \end{cases} \quad (14)$$

where $E = 4tf_y + 0.5(H - 2t)f_{ck}$

$$F = 0.5(B - t_w)(t_w - 2t)f_{ck} + 0.25(H - 2t) \times (t_w - B - 2t)f_{ck} - 2Btf_y - 0.3tf_y(H - t_w)$$

$$D = 2tf_y + 0.25(H - 2t)f_{ck}$$

$$P = 0.5(B - t_w)(t_w - 2t)f_{ck} - 2Btf_y - 0.25(H - 2t)(B - t_w)f_{ck} + 0.2(H - t_w)tf_y$$

Table 4
Positions of special-shaped cross-section centroidal axis and plastic neutral axis.

Section type	Loading angel ϑ	$B \times H \times t_w$	Centroidal axis h_0	Neutral axis h	abs($h-h_0$)/h
T-shaped	−90° (YYSY)	200 × 200 × 100	83.3	87.12	0.044
		300 × 300 × 100	110.0	114.28	0.038
		400 × 400 × 100	135.7	140.50	0.034
	0° (PXFB)	200 × 200 × 100	100.0	95.75	0.044
		300 × 300 × 100	150.0	146.20	0.026
		400 × 400 × 100	200.0	197.85	0.011
	90° (YYSL)	200 × 200 × 100	116.7	112.5	0.037
		300 × 300 × 100	190.0	185.7	0.023
		400 × 400 × 100	264.3	261.4	0.011
L-shaped	−45° (YYSY)	200 × 200 × 100	83.3	87.5	0.048
		300 × 300 × 100	110.0	112.51	0.022
		400 × 400 × 100	135.7	133.65	0.015
	135° (YYSL)	200 × 200 × 100	116.7	117.25	0.005
		300 × 300 × 100	190.0	184.5	0.030
		400 × 400 × 100	264.3	266.25	0.007

$$G = \left(B^2 - 2Bt + 2t^2\right) tf_y + Bt_w tf_y - t_w t^2 f_y + (H - t_w)(0.15B + 0.85t_w - 0.85t) tf_y + \frac{1}{16}(H - 2t)(B - t_w)^2 f_{ck} - \frac{1}{8}\left(t_w - 2t\right)(B - t_w)^2 f_{ck}$$

4.1.4. Comparison of sectional resistances at point C between FEM and simplified calculation

Table 5 is the comparison of sectional resistances of special-shaped CFST columns at point C between FEM and simplified calculation, where $N_{c,FEM}$ and $M_{c,FEM}$ are the FEM calculation values; N_{c1} and M_{c1} are the calculated values according to the simplified formulae in this paper. As can be seen from Table 5, the average values of $N_{c1}/N_{c,FEM}$ and $M_{c1}/M_{c,FEM}$ of T-shaped CFST columns are respectively 1.01 and 0.89(YYSY), 0.91 and 0.87 (YYSL), 0.90 and 0.87 (PXFB). And the average values of $N_{c1}/N_{c,FEM}$ and $M_{c1}/M_{c,FEM}$ of L-shaped CFST columns are respectively 0.96 and 1.03(YYSY), 0.96 and 0.91 (YYSL). Therefore, the simplified calculation formulae in this paper can slightly conservatively predict the resistances of special-shaped CFST columns at point C in characteristic directions (YYSY, YYSL and PXFB).

4.1.5. Second-order effect of special-shaped CFST columns

The second-order effect in the structure can be divided into two categories. The first type is the *P-Δ* effect caused by the vertical load in the sideway structure; the other one is the *P-δ* effect caused by the axial force of the member with the flexural deformation. For the general building structure, the above two second-order effects exist simultaneously, and the *P-Δ* effect can be obtained by general structural calculation software. Referring to domestic and foreign structural design specifications, such as JGJ 149-2017 [1], GB-50010 [28], ACI-318 [33] and Eurocode 2 [34], the *P-δ* effect of special-shaped CFST columns is considered by the method of amplifying the bending moment of the control section. That is, the design value of bending moment of the control section is multiplied by the eccentricity increasing coefficient η_θ to consider the *P-δ* effect (Eq. (15)), and the η_θ is calculated by the Eq. (16) based on the specification JGJ149−2017 [1].

$$\begin{cases} N \le N_u \\ \eta_\theta M \le M_u \end{cases} \quad (15)$$

Where N is the design value of sectional axial force; N_u is the sectional axial resistance; M is the design value of sectional bending moment; M_u is the sectional flexural resistance.

$$\begin{cases} \eta_\theta = 1 + \dfrac{1}{e_i/r_\theta}\left(l_0/r_\theta\right)^2 C \\ C = 1 - \left[0.232 + 0.604(e_i/r_\theta) - 0.106(e_i/r_\theta)^2\right] \\ r_\theta = \sqrt{\dfrac{I_\theta}{A}} \end{cases} \quad (16)$$

Where e is the initial eccentricity, $e = e_i + e_a$, $e_i = \dfrac{M_x + M_y}{N}$; e_a is the additional eccentricity, e_a = max (20 mm, 0.15 r_{min}), and r_{min} is the minimum radius of rotation of cross section. l_0 is the calculated length of column, determined according to the reference [17]; I_θ is the moment of inertia of the centroid axis x_θ-x_θ perpendicular to the direction of the eccentric compression (Fig. 16); A is the cross-sectional area. Note that both I_θ and A are calculated according to the section size, ignoring the combination of steel tube and concrete.

When $l_0/r_\theta \le 17.5$, the additional bending moment caused by the *P-δ* effect in the section of special-shaped CFST columns does not exceed 4.2% of the first-order bending moment of the section and the η_θ can be taken as 1.0 [1].

4.1.6. Comparison among experimental results, FEM results and the simplified calculation results of design method

Fig. 22 shows the comparison among experimental results, FEM results and simplified calculation results proposed in this paper, which reveals the simplified design formulae can conservatively predict the *N-M* correlation curve of special-shaped CFST columns.

4.2. Biaxial eccentric compression

For T-shaped and L-shaped CFST section with equal column limb (B=H) under biaxial eccentric compression, the loading angle ϑ can be studied from −90° to 90° due to the symmetry of the sections (Fig. 16). It is found that the column limb width-to-thickness ratio (B/t_w), steel to concrete ratio α, steel yield strength f_y, concrete compres- sive strength f_{ck}, loading angle ϑ, eccentricity e and section stiffening type have significant effects on the *N-M* correlation curves. Fig. 23 shows the *N-M*$_x$-*M*$_y$ correlation surface of T-shaped CFST column. The *N-M*$_x$-*M*$_y$ correlation surface is cut perpendicular to the vertical N axis to obtain the M_x-M_y correlation curves under different axial compression ratio n. Therefore, this section mainly studies the influence of column limb width-to-thickness ratio (B/t_w), axial compression ratio n, section stiffening type, steel to concrete ratio α, steel yield strength f_y, concrete compressive strength f_{ck} on M_x-M_y correlation curves.

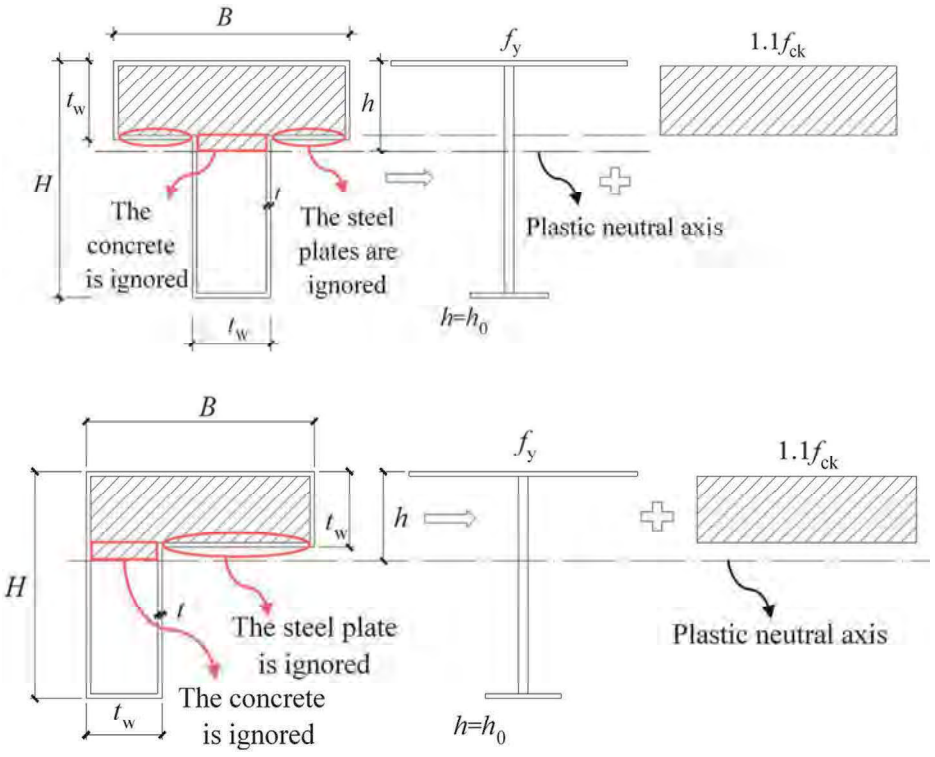

(a) YYSY

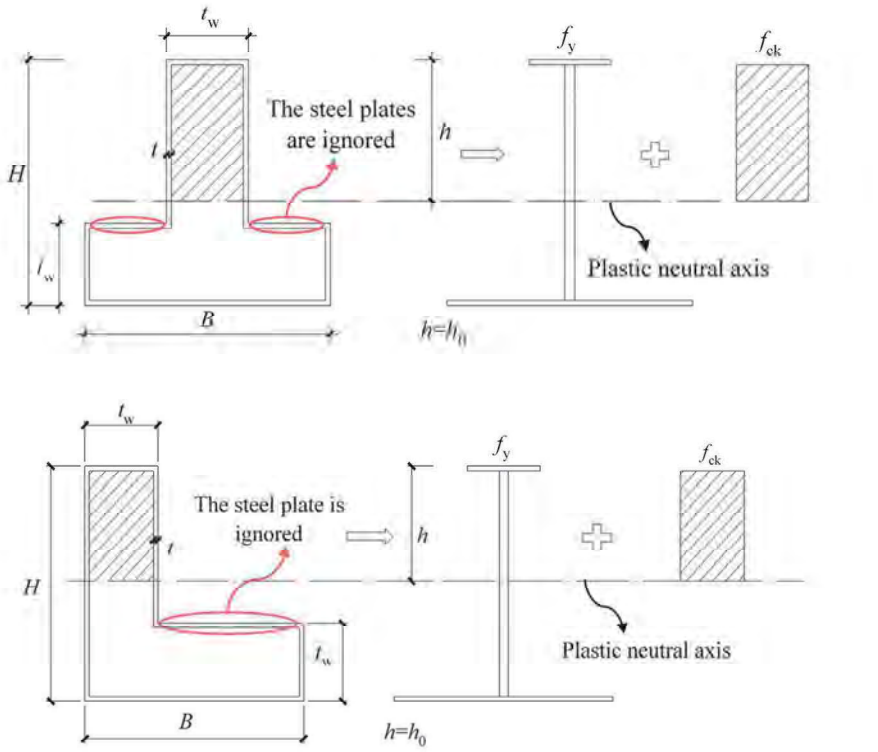

(b) YYSL

Fig. 21. Simplified model of stress distribution of T-shaped section at point C.

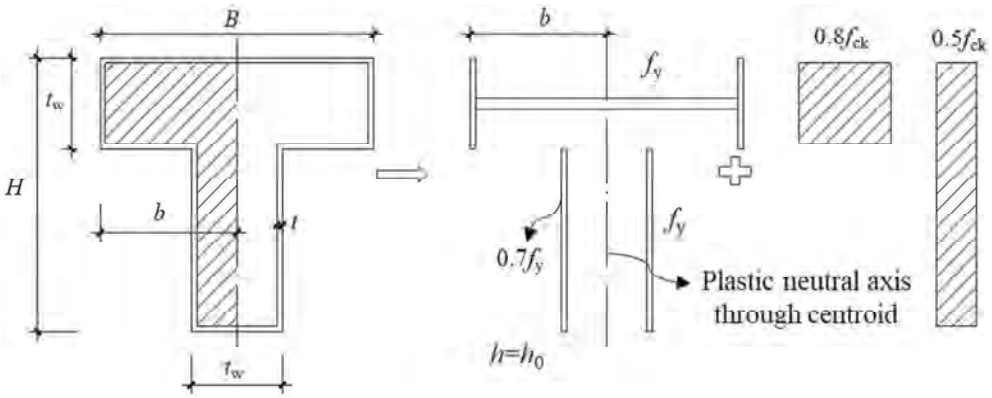

(c) PXFB

Fig. 21 (*continued*).

Table 5
Comparison of sectional resistance of special-shaped CFST column at point C.

Characteristic direction	T-shaped section ($B \times H \times t_w$)	Steel ratio α (%)	Steel tube f_y (MPa)	Concrete f_{ck} (MPa)	–	$N_{c1}/N_{c,FEM}$	$M_{c1}/M_{c,FEM}$
YYSY	200 × 200 × 100	4.8–11.7	235–345	20.1–40.0	Range	0.88–1.18	0.75–0.97
	300 × 300 × 100				Average value	1.01	0.89
	400 × 400 × 100				Standard deviation	0.105	0.071
YYSL	500 × 600 × 200				Range	0.72–1.16	0.78–0.97
	600 × 800 × 200				Average value	0.91	0.87
	800 × 800 × 200				Standard deviation	0.171	0.056
PXFB					Range	0.77–1.13	0.77–0.97
					Average value	0.90	0.87
					Standard deviation	0.092	0.056
Characteristic direction	L-shaped section ($B \times H \times t_w$)	Steel ratio α (%)	Steel tube f_y (MPa)	Concrete f_{ck} (MPa)	–	$N_{c1}/N_{c,FEM}$	$M_{c1}/M_{c,FEM}$
YYSY	200 × 200 × 100	4.8–11.7	235–345	20.1–40.0	Range	0.83–1.14	0.92–1.13
	300 × 300 × 100				Average value	0.96	1.03
	400 × 400 × 100				Standard deviation	0.085	0.067
YYSL					Range	0.82–1.10	0.82–0.99
					Average value	0.96	0.91
					Standard deviation	0.093	0.049

B× H× t_w is the T-shaped and L-shaped cross-sectional dimensions (in Fig. 8(f) and (g)). α is the area ratio of steel to concrete. f_{ck} is the concrete prismatic compressive strength. f_y is the steel yield strength. $M_{u,FEM}$ is the FEM calculation value. M_{u1} is the calculated value according to Eq. (5)-(10) in this paper. $N_{c,FEM}$ and $M_{c,FEM}$ are the FEM calculation values. N_{c1} and M_{c1} are the calculated values according to the Eq. (12)-(14) in this paper.

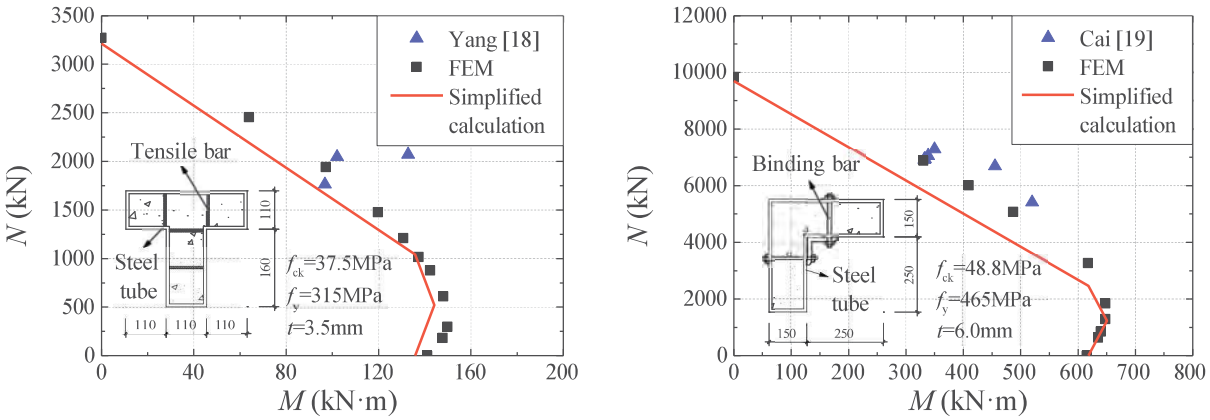

(a) Reference [21] (b) Reference [22]

Fig. 22. Comparison among experimental results, FEM results and simplified calculation results.

Fig. 24 shows the M_x-M_y correlation curves of T-shaped CFST column under different axial compression ratios n. It can be seen that the section stiffening type has effect on the values of the M_x-M_y correlation curves, but has almost no effect on the shape of M_x-M_y correlation curves, which is consistent with the conclusion of the L-shaped CFST column under biaxial eccentric compression test [19]. Combined with the FEM

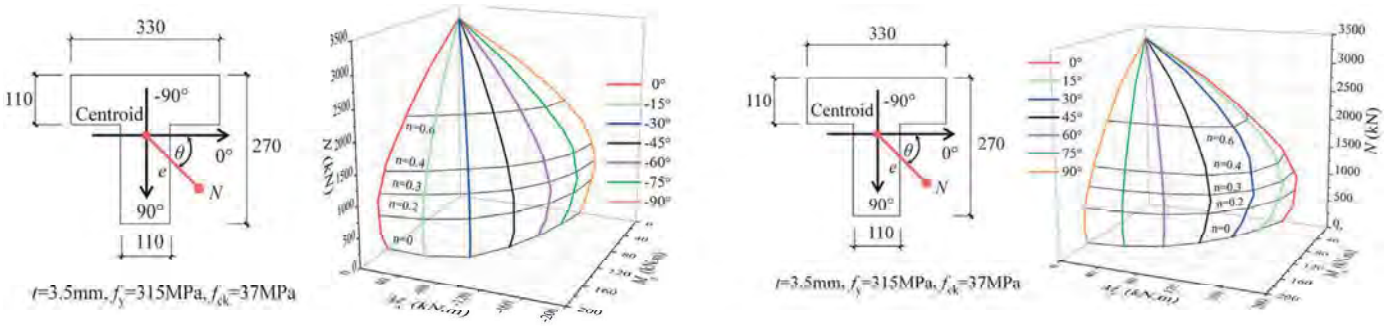

(a) Loading angle θ from 0° to -90°

(b) Loading angle θ from 0° to 90°

Fig. 23. N-M_x-M_y correlation surface.

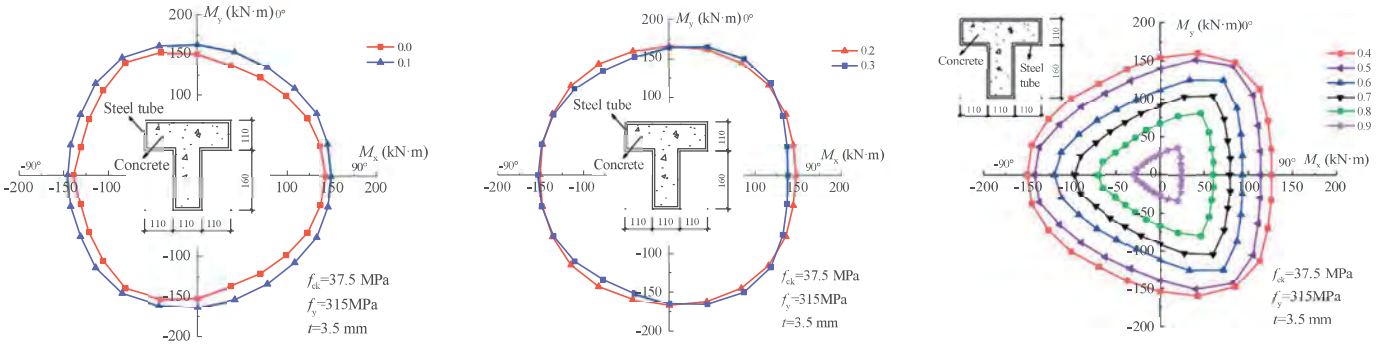

(a) Non-stiffened n=0.0-0.1

(b) Non-stiffened n=0.2-0.3

(c) Non-stiffened n=0.4-0.9

(d) Stiffened n=0.0-0.1

(e) Stiffened n=0.2-0.3

(f) Stiffened n=0.4-0.9

Fig. 24. M_x-M_y correlation curves of T-shaped CFST columns.

results and the conclusion of the reference [19], the steel-to -concrete ratio α, steel yield strength f_y and concrete strength f_{ck} have little effect on the shape of M_x-M_y correlation curves and can be neglected, while the column limb width-to-thickness ratio B/t_w and axial compression ratio n have significant effects on the shape of M_x-M_y correlation curves. Therefore, this section mainly studies the influence of column limb.

4.2.1. M_x-M_y correlation curves of T-shaped and L-shaped CFST sections

Since T-shaped and L-shaped CFST columns have similar regularity under different parameters of column limb width-to-thickness ratio B/t_w and axial compression ratio n, the T-shape CFST column is taken as an example here. Fig. 25 shows the influences of column limb width-to-thickness ratio B/t_w and axial compression ratio n on the M_x- M_y correlation curves of T-shaped CFST columns. For the case of low axial compression ratio ($n \leq 0.3$), as B/t_w decreases from 4 to 1.5, the shape of M_x-M_y correlation curves gradually changes from ellipse to circle. For the case of high axial compression ratio (n ℕ 0.3), as the axial compression ratio n increases, the shape of M_x-M_y correlation curves gradually changes from ellipse to triangle. In order to check the resistances of special-shaped CFST columns under biaxial eccentric compression, the M_x-M_y correlation curves of T-shaped and L-shaped CFST columns are fitted by the Eq. (17) based on a large number of parametric analysis results (1872 FEM results).

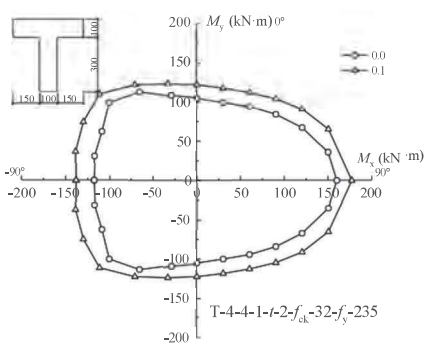

(a) T-400-400-100-n=0.0-0.1

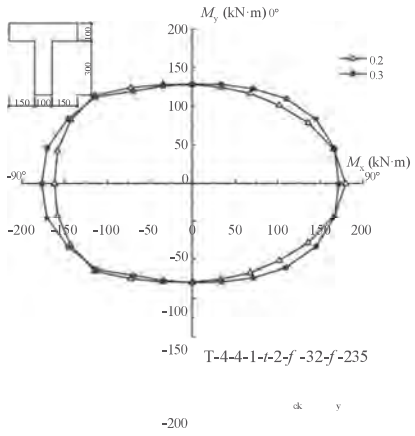

(b) T-400-400-100-n=0.2-0.3

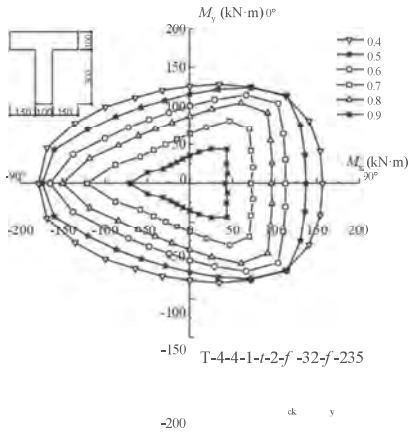

(c) T-400-400-100-n=0.4-0.9

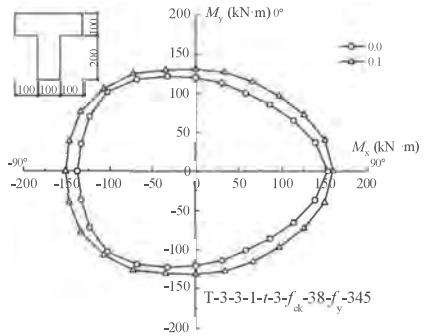

(d) T-300-300-100-n=0.0-0.1

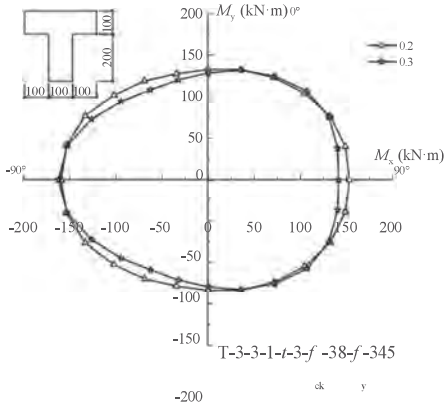

(e) T-300-300-100-n=0.2-0.3

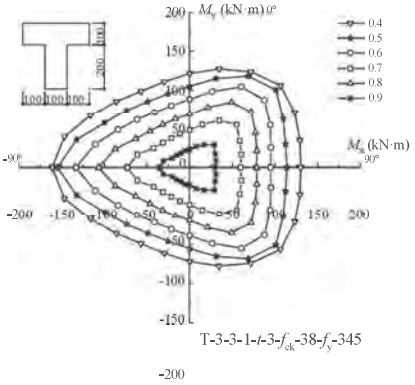

(f) T-300-300-100-n=0.4-0.9

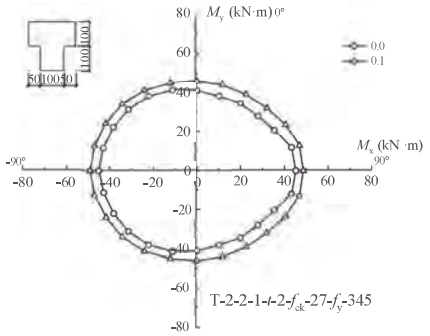

(g) T-200-200-100-n=0.0-0.1

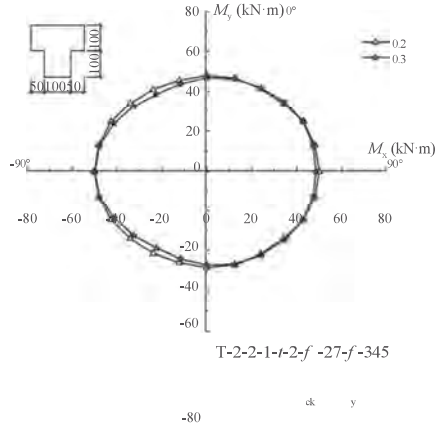

(h) T-200-200-100-n=0.2-0.3

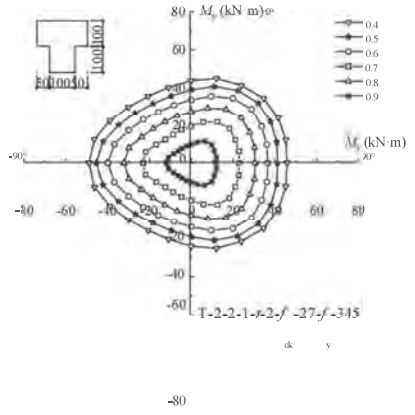

(i) T-200-200-100-n=0.4-0.9

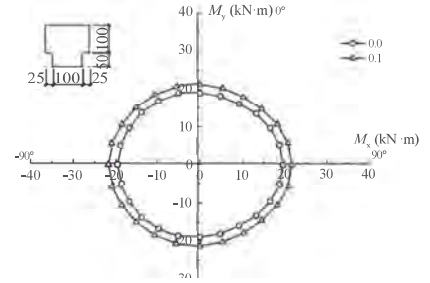

50 100

)

50 100

)

(j) T-150-150-100-n=0.0-0.1 (k) T-150-150-100-n=0.2-0.3 (l) T-150-150-100-n=0.4-0.9

Fig. 25. Influence of B/t_w and n on M_x-M_y related curve of T-shaped CFST columns.

Table 6
Resistance coefficients α_1 and α_2 of T-shaped CFST columns under biaxial eccentric compression.

Coefficients α_1 and α_2 of T-shaped CFST columns with equal column limbs ($B = H$)											
Loading angel ϑ	n	0		0.1		0.2		0.3		0.4	
90°–0°	B/t_w	α_1	α_2	α_1	α_2	α_1	α_2	α_1	α_2	α_1	α_2
	1.5	1.50	2.00	1.60	2.00	1.70	2.00	1.80	2.00	2.00	2.00
	2.0	1.40	2.00	1.72	2.00	2.00	2.00	2.40	2.00	3.40	2.00
	2.5	1.30	2.00	1.50	2.00	2.10	2.00	2.80	2.00	4.00	2.00
	3.0	1.30	1.80	1.60	2.00	2.60	2.00	4.00	2.00	6.20	2.00
	3.5	1.30	1.60	1.66	1.70	2.00	2.00	3.40	2.00	5.40	2.00
	4.0	1.30	2.00	1.80	2.00	1.80	2.00	3.20	2.00	4.80	2.00
	n	0.5		0.6		0.7		0.8		0.9	
	B/t_w	α_1	α_2	α_1	α_2	α_1	α_2	α_1	α_2	α_1	α_2
	1.5	2.40	2.00	2.40	2.00	2.40	2.00	2.40	2.00	2.40	2.00
	2.0	4.60	2.00	5.60	2.00	6.80	2.00	7.60	2.00	8.80	2.00
	2.5	7.20	2.00	9.80	2.00	11.00	2.00	11.40	2.00	12.00	2.00
	3.0	11.00	2.00	14.00	2.00	15.20	2.00	15.20	2.00	15.20	2.00
	3.5	11.00	2.00	14.00	2.00	15.20	2.00	15.20	2.00	15.20	2.00
	4.0	11.00	2.00	14.00	2.00	15.20	2.00	15.20	2.00	15.20	2.00
Loading angel ϑ	n	0		0.1		0.2		0.3		0.4	
−90°–0°	B/t_w	α_1	α_2	α_1	α_2	α_1	α_2	α_1	α_2	α_1	α_2
	1.5	2.20	1.80	2.00	1.80	1.80	1.80	1.64	1.80	1.64	1.80
	2.0	2.88	1.80	2.50	1.80	2.00	1.80	1.70	1.80	1.50	1.80
	2.5	3.10	1.80	2.80	1.80	2.20	1.80	1.68	1.80	1.50	1.80
	3.0	4.20	1.80	3.40	1.80	2.30	1.80	1.64	1.80	1.48	1.80
	3.5	5.20	1.80	4.60	1.80	3.00	1.80	2.00	1.80	1.50	1.80
	4.0	6.80	1.80	6.00	1.80	4.20	1.80	3.00	1.80	1.92	1.80
	n	0.5		0.6		0.7		0.8		0.9	
	B/t_w	α_1	α_2	α_1	α_2	α_1	α_2	α_1	α_2	α_1	α_2
	1.5	1.64	1.80	1.64	1.80	1.52	1.80	1.36	1.80	1.26	1.80
	2.0	1.26	1.80	1.12	1.80	1.00	1.80	1.00	1.80	0.80	1.80
	2.5	1.20	1.80	1.00	1.80	0.80	1.80	0.80	1.80	0.80	1.80
	3.0	1.12	1.80	0.90	1.80	0.80	1.80	0.80	1.80	0.80	1.80
	3.5	1.12	1.80	0.90	1.80	0.80	1.80	0.70	1.80	0.68	1.80
	4.0	1.40	1.80	0.90	1.80	0.80	1.80	0.60	1.80	0.60	1.80

$$\left(\frac{M_x}{M_{0x}}\right)^{\alpha_1} + \left(\frac{M_y}{M_{0y}}\right)^{\alpha_2} \leq 1 \qquad (17)$$

Where M_x and M_y are the sectional bending moments; M_{0x} and M_{0y} are the bending capacities of the characteristic directions (YYSY, YYSL and PXFB) under the corresponding axial force N, which are calculated according to the resistance of special- shaped CFST columns under uniaxial eccentric compression ac- cording to section 4.1. The coefficients α_1 and α_2 are determined

according to the column limb width-to-thickness ratio B/t_w and axial compression ratio n in Tables 6-7, which are linearly interpolated.

4.2.2. Comparison of sectional M_x-M_y correlation curves between FEM results and simplified calculation results

Figs. 26 shows comparison of sectional M_x-M_y correlation curves of special-shaped CFST columns under biaxial eccentric compression between FEM results and simplified calculation results determined by Eq. (17). It can be seen that the Eq. (17) agrees well with the FEM results, and the fitting formula is overall conservative.

5. Conclusions

The following conclusions can be drawn based on the study.

(1) According to the existing experimental results of special-shaped CFST columns under pure bending and eccentric compression, the finite element (FE) software ABAQUS is used to established FE models. The FE models agree well with the experimental results, which verifies the accuracy of the FE models.

Table 7

Resistance coefficients α_1 and α_2 of L-shaped CFST columns under biaxial eccentric compression.

Coefficients α_1 and α_2 of L-shaped CFST columns with equal column limbs ($B = H$)											
Loading	n	0		0.1		0.2		0.3		0.4	
angel ϑ	B/t_w	α_1	α_2	α_1	α_2	α_1	α_2	α_1	α_2	α_1	α_2
90°-0°	1.5	2.60	1.80	2.40	1.80	2.38	1.80	2.30	1.80	2.00	1.80
	2.0	2.60	1.80	2.20	1.80	2.00	1.80	1.72	1.80	1.60	1.80
	2.5	2.40	1.80	2.20	1.80	1.80	1.80	1.50	1.80	1.20	1.80
	3.0	2.10	1.80	1.86	1.80	1.80	1.80	1.50	1.80	1.00	1.80
	3.5	2.10	1.80	2.00	1.80	1.40	1.80	1.10	1.80	0.90	1.80
	4.0	1.90	1.80	1.70	1.80	1.20	1.80	1.00	1.80	1.00	1.60
	n	0.5		0.6		0.7		0.8		0.9	
	B/t_w	α_1	α_2	α_1	α_2	α_1	α_2	α_1	α_2	α_1	α_2
	1.5	1.80	1.80	1.70	1.80	1.70	1.80	1.70	1.80	1.70	1.80
	2.0	1.40	1.80	1.30	1.80	1.30	1.80	1.30	1.80	1.30	1.80
	2.5	1.10	1.80	1.00	1.80	1.00	1.80	1.00	1.80	1.00	1.50
	3.0	1.00	1.60	1.00	1.60	1.00	1.50	1.00	1.40	1.00	1.30
	3.5	1.00	1.60	1.00	1.40	1.00	1.40	1.00	1.40	1.00	1.30
	4.0	1.00	1.30	1.00	1.30	1.00	1.40	1.00	1.40	1.00	1.20
Loading	n	0		0.1		0.2		0.3		0.4	
angel ϑ	B/t_w	α_1	α_2	α_1	α_2	α_1	α_2	α_1	α_2	α_1	α_2
−90°-0°	1.5	2.40	2.00	2.44	2.00	2.48	2.00	2.50	2.00	2.70	2.00
	2.0	1.90	2.00	2.00	2.00	2.20	2.00	2.50	2.00	3.20	2.00
	2.5	1.60	2.00	1.80	2.00	2.00	2.00	2.40	2.00	3.80	2.00
	3.0	1.10	2.00	1.40	2.00	2.00	2.00	3.00	2.00	4.00	2.00
	3.5	1.10	2.00	1.40	2.00	1.60	2.00	2.40	2.00	3.80	2.00
	4.0	1.10	2.00	1.30	2.00	1.60	2.00	2.60	2.00	3.80	2.00
	n	0.5		0.6		0.7		0.8		0.9	
	B/t_w	α_1	α_2	α_1	α_2	α_1	α_2	α_1	α_2	α_1	α_2
	1.5	2.80	2.00	2.90	2.00	3.00	2.00	3.20	2.00	3.30	2.00
	2.0	4.00	2.00	4.20	2.00	4.00	2.00	2.60	2.00	2.50	2.00
	2.5	4.00	2.00	5.40	2.00	4.20	2.00	3.40	2.00	2.60	2.00
	3.0	5.40	2.00	8.80	2.00	9.80	2.00	6.80	2.00	6.00	2.00
	3.5	4.90	2.00	7.80	2.00	9.60	2.00	5.80	2.00	4.80	2.00
	4.0	5.60	2.00	8.80	2.00	9.80	2.00	6.80	2.00	3.80	2.00

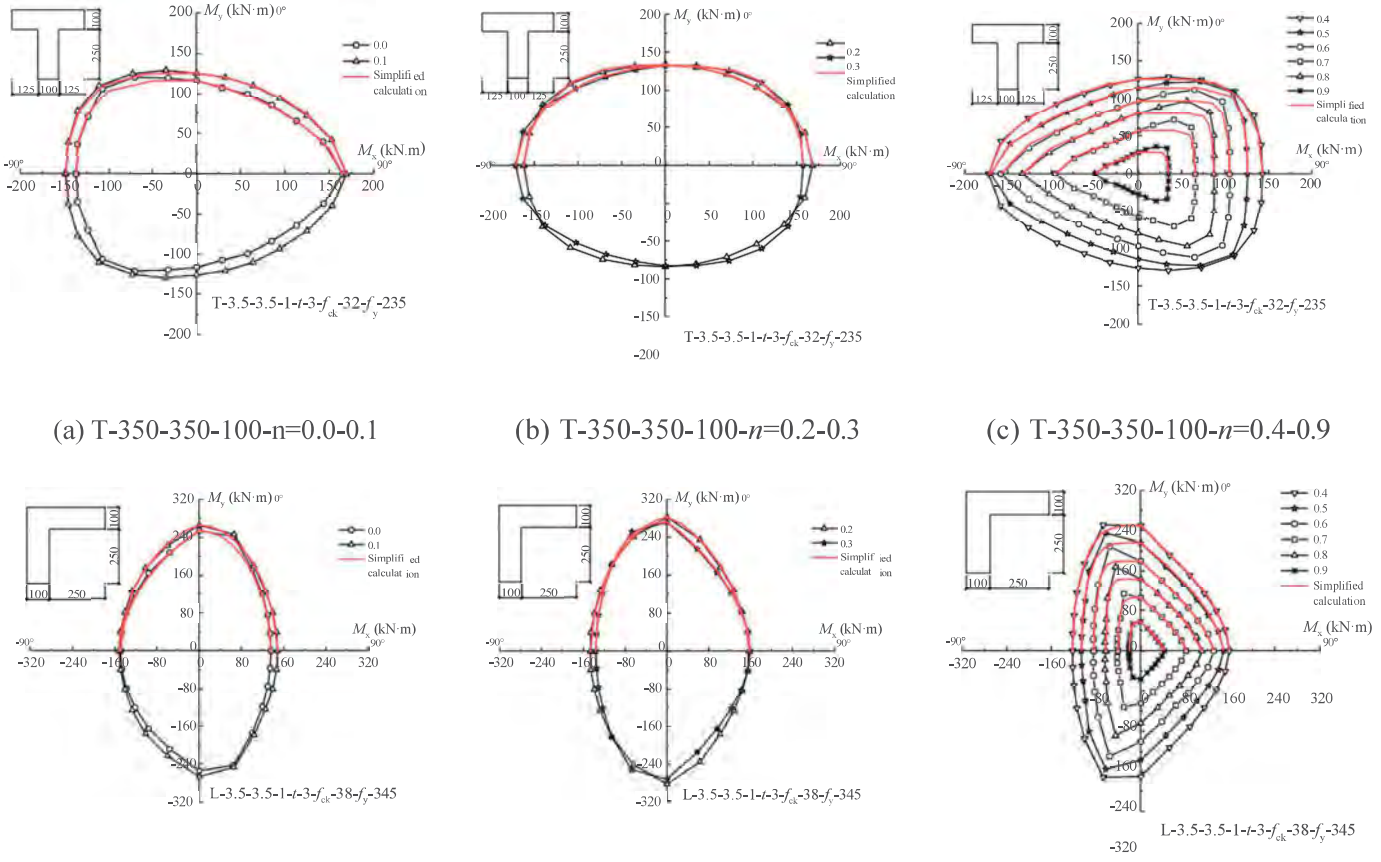

(a) T-350-350-100-n=0.0-0.1 (b) T-350-350-100-*n*=0.2-0.3 (c) T-350-350-100-*n*=0.4-0.9

(d) L-350-350-100-*n*=0.0-0.1 (e) L-350-350-100-n=0.2-0.3 (f) L-350-350-100-n=0.4-0.9

Fig. 26. Comparison of sectional M_x-M_y correlation curves of T-shaped and L-shaped CFST columns.

(2) According to the Mises stress distributions calculated by the FE model, the simplified models of the sectional stress distributions were proposed for the simplified calculation, and the corresponding simplified calculation formulae were derived. The simplified calculation formulae can accurately predict the flexural resistances of special-shaped CFST columns in the characteristic direction (YYSY, YYSL and PXFB).

(3) The effects of parameters such as section stiffening measures, loading angel ϑ, column limb width-to-thickness ratio B/t_w, steel ratio α, material strength (f_y, f_{ck}), eccentricity and axial compression ratio n on the mechanical properties of columns under eccentric compression were analyzed. On this basis, a simplified calculation formula for the sectional *N*-*M* correlation curve of special-shaped CFST columns under uniaxial eccentric compression was proposed, which can conservatively predict the *N*-*M* correlation curve. The study also found that the steel ratio α, material strength (f_y, f_{ck}) and section stiffening measures have little effect on the shape of the M_x-M_y correlation curves, which can be neglected, while the column limb width-thickness ratio B/t_w and axial compression ratio n have significant influence on the shape of the M_x-M_y corre- lation curves. A formula for checking the resistances of special-shaped CFST columns under biaxial eccentric com- pression was proposed based on 1872 FE models analysis re- sults, which is generally conservative.

Declaration of Competing Interest

None.

Acknowledgments

This research is supported by Foundation of Key Laboratory of Structures Dynamic Behavior and Control (Ministry of Education) in Harbin Institute of Technology (Grant No. 30620180333), National Natural Science Foundation of China (Grant No. 51878098), National Key Research and Development Program of China (Grant No. 2016YFC0701201, 2017YFC0703805) and Natural Science Foundation Project of CQ CSTC (cstc2019jcyj-msxmX0580).

References

[1] JGJ 149–-2017, Technical specification for concrete structures with specially shaped columns, Architecture Industrial Press of China, Beijing, 2006 (in Chinese).

[2] M. Joaquin, Design aids for L-shaped reinforced concrete columns, ACI Struct. J. 76 (49) (1979) 1197–1216.

[3] T. Cheng, H. Thomas, T-shaped reinforced concrete members under biaxial bending and axial compression, ACI Struct. J. 86 (4) (1989) 2576–2595.

[4] P. Mahadevappa Mallikarjuna, Computer aided analysis of reinforced concrete columns subjected to axial compression and bending - I L-shaped sections, Comput. Struct. 44 (5) (1992) 1121–1138.

[5] P. Mahadevappa Mallikarjuna, Computer-aided analysis of reinforced concrete column subjected to axial compression and bending. Part II: T-shaped sections, Comput. Struct. 53 (6) (1994) 1317–1356.

[6] C. Dundar, B. Sahin, Arbitrarily shaped reinforced concrete members subjected to biaxial bending and axial load, Comput. Struct. 49 (4) (1993) 643–662.

[7] C.Y. Yau, S.L. Chan, A.K.W. So, Biaxial bending design of arbitrarily shaped reinforced concrete column, ACI Struct. J. 90 (3) (1993) 269–279.

[8] Z.Y. Lin, Z.Y. Shen, J.H. Luo, Hysteretic behavior of concrete-filled L-section steel tubular columns under cyclic loading, Prog. Steel Build. Struct. 11 (2) (2009) 12–17(in Chinese).

[9] Y.L. Yang, H. Yang, S.M. Zhang, Compressive behavior of T-shaped concrete filled steel tubular columns, Int. J. Steel Struct. 10 (4) (2010) 419–430.

[10] Z.L. Zuo, J. Cai, C. Yang, et al., Axial load behavior of L-shaped CFST stub columns with binding bars, Eng. Struct. 37 (2012) 88–98.

[11] Y.Q. Tu, Y.F. Shen, P. Li, Behaviour of multi-cell composite T-shaped concrete-filled steel tubular columns under axial compression, Thin-Walled Struct. 85 (2014) 57–70.

[12] Y.Q. Tu, Y.F. Shen, Y.G. Zeng, et al., Hysteretic behavior of multi-cell T-shaped concrete-filled steel tubular columns, Thin-Walled Struct. 85 (2014) 57–70.

[13] Z.L. Zuo, J. Cai, Q.J. Chen, et al., Performance of T-shaped CFST stub columns with binding bars under axial compression, Thin-Walled Struct. 129 (2018) 183–196.

[14] J.C. Zhang, Z.Y. Shen, Z.Y. Lin, et al., Experimental research on seismic behavior of concrete-filled L-shaped steel tubular frames, J. Build. Struct. 31 (8) (2010) 1–7(in Chinese).

[15] Y.L. Yang, Y.Y. Wang, S.M. Zhang, Experimental research on seismic behavior of T-shaped concrete-filled steel tube columns with reinforcement stiffeners, J. Build. Struct. 33 (4) (2012) 104–112(in Chinese).

[16] X.G. Liu, C.Z. Xu, J.P. Liu, Y.L. Yang, Research on special-shaped concrete-filled steel tubular columns under axial compression, J. Constr. Steel Res. 147 (2018) 203–223.

[17] GB 50936–2014, Technical Code for Concrete Filled Steel Tubular Structures, Architecture Industrial Press of China, Beijing, 2014 (in Chinese).

[18] Y.L. Yang, Y.Y. Wang, F. Fu, et al., Static behavior of T-shaped concrete-filled steel tubular columns subjected to concentric and eccentric compressive loads, Thin-Walled Struct. 95 (2015) 374–388.

[19] Z.L. Zuo, J. Cai, C. Yang, et al., Eccentric load behavior of L-shaped CFT stub columns with binding bars, J. Constr. Steel Res. 72 (2012) 105–118.

[20] S.B. Liu, L.H. Xu, F. Wen, Experimental investigation of flexural behavior of T-section concrete-filled steel tubular composite members, J. Wuhan Univ. Technol. 30 (11) (2008) 108–112(in Chinese).

[21] Q. Yu, Z. Tao, W. Liu, Z.B. Chen, Analysis and calculations of steel tube confined concrete (STCC) stub columns, J. Constr. Steel Res. 66 (2010) 53–64.

[22] L.H. Han, G.H. Yao, Z. Tao, Performance of concrete-filled thin-walled steel tubes under pure torsion, Thin-Walled Struct. 45 (2007) 24–36.

[23] J.C. Liu, Y.L. Yang, J.P. Liu, X.H. Zhou, Experimental investigation of special-shaped concrete-filled steel tubular column to steel beam connections under cyclic loading, Eng. Struct. 151 (2017) 68–84.

[24] D. Kueres, A. Stark, M. Herbrand, et al., Finite element simulation of cosncrete with a plastic damage model - basic studies on normal strength concrete and UHPC, Bauingenieur 90 (2015) 252–264.

[25] T. Yu, J.G. Teng, Y.L. Wong, S.L. Dong, Finite element modeling of confined concrete-II: plastic-damage model, Eng. Struct. 32 (2010) 680–691.

[26] L.H. Han, Flexural behaviour of concrete-filled steel tubes, J. Constr. Steel Res. 60 (2) (2004) 313–337.

[27] L.H. Han, H. Lu, G.H. Yao, et al., Further study on the flexural behaviour of concrete-filled steel tubes, J. Constr. Steel Res. 62 (6) (2006) 554–565.

[28] GB 50010–2010, Code for Design of Concrete Structures, Architecture Industrial Press of China, Beijing, 2010 (in Chinese).

[29] F.W. Lu, S.P. Li, D.W. Li, et al., Flexural behavior of concrete filled non-uni-thickness walled rectangular steel tube, J. Constr. Steel Res. 63 (8) (2007) 1051–1057.

[30] W.M. Gho, D. Liu, Flexural behaviour of high-strength rectangular concrete-filled steel hollow sections, J. Constr. Steel Res. 60 (11) (2004) 1681–1696.

[31] R. Wang, L.H. Han, J.G. Nie, X.L. Zhao, Flexural performance of rectangular CFST members, Thin-Walled Struct. 79 (2) (2014) 154–165.

[32] G.C. Li, D. Liu, Z.J. Yang, C.Y. Zhang, Flexural behavior of high strength concrete filled high strength square steel tube, J. Constr. Steel Res. 128 (2017) 732–744.

[33] ACI 318–11, Building Code Requirements for Structural Concrete and Commentary [S], American Concrete Institute, Farmington Hills, MI, 2011.

[34] British Standards institution, Eurocode 2: Design of Concrete Structures: Part 1–1: General Rules and Rules for Buildings[S], British Standards institution, 2004.

[35] Y.H. Yan, H.J. Liang, Y.Y. Lu, et al., Behaviour of RC columns strengthened with SCC-filled steel tubes under cyclic loading, Eng. Struct. 199 (2019), 109603.

[36] Y.H. Yan, H.J. Liang, Y.Y. Lu, et al., Axial behavior of slender RC square columns strengthened with circular steel tube and sandwiched concrete jackets, Eng. Struct. 179 (2019) 423–437.

[37] Y.L. Yang, Mechanical Behaviors of T-Shaped Composite Columns, Harbin Institute of Technology, 2011 PhD thesis. (in Chinese).

[38] H. Song, Research on Mechanical Behavior of Multi-Cell Special-Shaped Concrete-Filled Steel Tubular Stub Columns Under Axial Compression, Chongqing Univ, 2017 Master's thesis. (in Chinese).